Late Mesoproterozoic Deformation of SW Amazonia (Rondônia, Brazil): Geochronological and Structural Evidence for Collision with Southern Laurentia

E. Tohver,[1] *B. A. van der Pluijm, J. E. Scandolâra,*[2,3] *and E. J. Essene*

Department of Geological Sciences, University of Michigan, Ann Arbor, Michigan 48109-1063, U.S.A. (e-mail: etohver@umich.edu)

ABSTRACT

Proposed assembly of the Rodinia supercontinent in the late Mesoproterozoic involved the collision of the Amazon craton with some portion of the southern or eastern margin of cratonic North America. Previously reported paleomagnetic data from the SW Amazon craton suggest a paleogeographic link between "Grenvillian" deformation of the SW Amazon craton and late Mesoproterozoic tectonometamorphism in southern Laurentia. A structural, geochronological, and petrological investigation of the western Amazon basement rocks (Rondônia, Brazil) was carried out in order to document evidence of a Grenvillian collision connecting the Amazon to Laurentia. Integration of $^{40}Ar/^{39}Ar$ data and feldspar thermometry data from regionally extensive strike-slip mylonitic shear zones (Ji-Paraná shear zone network) indicates that deformation took place at 450°–550°C between 1.18 and 1.15 Ga. An older, ca. 1.35-Ga event found exclusively in less-deformed basement rocks is interpreted as recording cooling from an earlier metamorphic episode (650°–800°C indicated by feldspar thermometry) unrelated to the Grenville collision. The style of deformation in the SW Amazon craton contrasts with that observed in southern Laurentia, where extensive crustal thickening accommodated by deep-seated thrust sheets resulted in widespread thermal resetting of isotopic systems during exhumation and postorogenic cooling. In contrast, the predominantly strike-slip activity observed in the Amazon resulted in age resetting through strain-induced recrystallization, not regional-scale thermal resetting. Consequently, the ages recorded by hornblende in the SW Amazon craton are slightly older than the cooling ages preserved in southern Laurentia. Differences in structural style and geochronological record are interpreted as indicative of an exhumed, asymmetric crustal structure similar to that of modern orogens.

Online enhancements: appendixes.

Introduction

The North American Grenville Province, which stretches from the Llano Uplift area of central Texas to northeastern Labrador, has long been recognized as an exhumed zone of middle to deep crustal orogenesis based on structural geology, the resetting of isotopic age systems, and high *PT* conditions reflective of middle to deep crustal equilibration for rocks now exposed at the surface (Easton 1992; Mezger et al. 1993; Rivers 1997; Davidson 1998; Mosher 1998). Seismic profiles of the Canadian portion of this belt highlight the presence of shallowly dipping structures, interpreted as imbricated thrust sheets emplaced during a major collisional event (Rivers et al. 1989; White et al. 1994). The Rodinia hypothesis builds on these observations to suggest that the Grenville orogeny records the amalgamation of a supercontinent through the collision of Laurentia with other cratons, with the Baltic, Amazon, and Kalahari cratons advanced as the most likely candidates (Hoffman 1991; Dalziel et al. 2000; Tohver et al. 2002).

Evidence for the respective roles of Baltica, the Kalahari, and Amazonia within the Rodinia framework is of variable quality. The case for Baltica

Manuscript received February 3, 2004; accepted November 19, 2004.

[1] Author for correspondence; present address: Instituto de Geociências, Universidade de São Paulo, Rua do Logo 562, Cidade Universitária, 05508-080 São Paulo, SP, Brazil.

[2] Companhia de Pesquisa de Recursos Minerais, Avenida Lauro Sodré 2561, Porto Velho, RO, Brazil 78904-300.

[3] Present address: Instituto de Geociências, Universidade de Brasília, 70910-900 Brasília, DF, Brazil.

[The Journal of Geology, 2005, volume 113, p. 309–323] © 2005 by The University of Chicago. All rights reserved. 0022-1376/2005/11303-0004$15.00

seems the most compelling on the basis of both paleomagnetic evidence and geological observations. The paleomagnetically derived position of Baltica relative to Laurentia is constrained by matching apparent polar wander paths (APWPs) for the period 1.05–0.95 Ga for both continents (Piper 1987; Weil et al. 1998) or by comparing individual poles from both cratons (Hartz and Torsvik 2002). Both analyses point to a location for Baltica adjacent to the northeasternmost Grenville Province, although the orientation of Baltica differs in the respective reconstructions. Geological correlations have also been cited in support of the northeastern position for Baltica near either Labrador or Greenland (Gower et al. 1990; Hoffman 1991; Cawood et al. 2001).

The paleogeographic position of Amazonia is constrained by a paleomagnetic pole for the earliest portion (ca. 1.2 Ga) of the Grenville interval (Tohver et al. 2002). By comparing the latitude and orientation of the Amazon craton with the paleogeographic drift of Laurentia for the 1.35–1.15-Ga interval, Tohver et al. (2002) proposed a tectonic link between Amazonia and southern Laurentia at ca. 1.2 Ga. The possibility of a collision between the two cratons at this time is compatible with known constraints on the timing of major deformation in the Llano region, which occurred between 1.24 and 1.10 Ga (Walker 1992). However, given the lack of other paleomagnetic data from Amazonia for the remainder of the Grenville interval, there is no constraint on the relative paleolongitude of these two cratons. Thus, for now, the assessment of the proposed Amazon-Llano collision must be made on the basis of geological evidence for a collision from both cratons. Although isotopic similarities between the SE Appalachian basement and the SW Amazonian craton support a paleogeographic link between these two cratons at a later interval (ca. 1.0 Ga, according to Loewy et al. 2003; 1145–1075 Ma according to Tohver et al. 2004*a*), the "Grenvillian" deformation history of the SW Amazon presumably caused by the collision has not been documented, in contrast with the well-studied Grenvillian history of southern Laurentia (e.g., Bristol and Mosher 1989; Walker 1992; Roback 1996; Carlson and Schwarze 1997; Mosher 1998; Grimes and Mosher 2003; Grimes and Copeland 2004).

The proposed collision between Amazonia and southern Laurentia contrasts with an earlier proposal that identified the Kalahari craton as the missing "southern continent" (Dalziel et al. 2000). However, the case for the Kalahari is weakened by direct comparison of paleogeography through paleomagnetism as well as disparities in the geological record from the Grenvillian belts of both cratons. Comparison of the APWPs from the Kalahari and Laurentian cratons demonstrates that a common geological history is plausible only for the period after 1.06 Ga (Powell et al. 2001). This analysis reveals a latitudinal separation of 30° ± 14° for times as late as 1.11 Ga, which is difficult to reconcile with the 1.24–1.10 Ga collisional scenario documented for southern Laurentia (Walker 1992). New, high-precision geochronological constraints on the age of paleomagnetic reversals recorded in the Umkondo Province of the Kalahari craton reported by Hanson et al. (2004) allow detailed correlation with Laurentian paleopoles known to be of the same geomagnetic polarity. In addition to confirming the ca. 3000-km distance between the Kalahari and southern Laurentia, the new constraints indicate a 90° misorientation between the Grenville Province of Laurentia and the Grenvillian Namaqua-Natal belt of the Kalahari craton, convincing proof that these belts cannot have originated from a collision between their respective cratons. Geological observations also reveal age discrepancies between deformation of southern Laurentia and Grenvillian deformation of the Kalahari craton. The timing of peak metamorphism varies somewhat in the Namaqua-Natal belt, with U-Pb zircon ages from Namaqua (westernmost extent) yielding ages of 1.07–1.13 Ga, slightly older than the 1.06-Ga age reported from the easternmost, Natal section of the belt (Jacobs et al. 1993). The age of metamorphic rims on zircon from high-grade rocks of East Antarctica, once contiguous to the eastern end of the Namaqua-Natal belt, was established as 1.09–1.05 Ga on the basis of SHRIMP analysis of zircon (Jacobs et al. 2003). These combined constraints suggest that the collisional event responsible for high-grade metamorphism in the Kalahari craton is considerably younger than the similar high-grade deformation of southern Laurentia at 1.24–1.10 Ga (Walker 1992). At the time of Kalahari peak metamorphism, deformation in southern Laurentia was limited to late strike-slip motion and thrusting during a greenschist/lower amphibolite facies event in west Texas (Soegaard and Callahan 1994; Bickford et al. 2000; Grimes and Copeland 2004).

The proposed position of the Amazon craton against the southernmost extent of the North American Grenville Province relies on a reconstruction of the tectonometamorphic history of the restored "greater" Grenville mobile belt that marks the collision between the two cratons. In this article, we present new geochronological, petrologi-

cal, and structural observations of the late Mesoproterozoic deformation of the SW Amazon craton. Geochronological data from exhumed mountain belts may reflect different aspects of orogenic history: the age of crystallization from magmatic or peak metamorphic conditions, the age of cooling through a mineral's blocking temperature for the retention of radiogenic daughter products, and the age of deformation in cases where strain-induced recrystallization took place at or above peak metamorphic temperatures. Thus, the geological significance of geochronological data depends on the regional pressure-temperature-time and deformational history, precluding a simple comparison of numerical age data from different portions of a belt. With this caveat, we conclude that the Grenvillian ages reported from the Amazon are true deformation ages, in contrast with ages reported from southern Laurentia that probably record cooling from peak metamorphic conditions or some other portion of the postcollisional history of exhumation. The collision between the Amazon and southern Laurentia is inferred to have created an asymmetric orogenic structure, accommodated by widespread crustal thickening on one continent (Laurentia), while the other continent (Amazonia) was marked by pervasive strike-slip faulting.

SW Amazon Regional Geology

Two cratonic masses comprise the Amazon craton along its SW margin: basement rocks of the Amazon craton itself and a subcontinental-sized block known as the Paragua craton (Litherland et al. 1989; Tassinari et al. 2000). Suturing of these cratons is recorded by the 1.0-Ga Nova Brasilândia metasedimentary belt (fig. 1), which was accompanied by high-grade thrusting and transpressional tectonics (Tohver et al. 2004*b*). North of this belt, the granitoid basement rocks of the SW Amazon craton record a protracted history of plutonism and metamorphism throughout the Mesoproterozoic (Bettencourt et al. 1999; Payolla et al. 2002). The Roosevelt Province, a 1.55-Ga domain within the SW Amazon craton, is dominated by low-grade, undeformed volcanosedimentary rocks, thus forming a northeastern limit to high-grade basement reactivation. To the north of the Nova Brasilândia metasedimentary belt, the polyphase nature of the Amazon basement rocks prevents the recognition of clear boundaries on the sole basis of different age provinces (Bettencourt et al. 1999). Major geological contacts are the result of tectonic juxtaposition, which has obscured many of the original intrusive relations (Tohver et al. 2005).

The youngest ductile deformation that affected these rocks is manifested in a wide network of amphibolite-grade shear zones, mapped as the Ji-Paraná shear zone (JPSZ) network by Scandolâra et al. (1999). The JPSZ is recognizable on regional RADARSAT images as large-scale lineaments that extend over hundreds of kilometers and transect the Amazon basement. Two trends mark the JPSZ along its full extent, a strongly deformed SE portion marked by NNW trends and a less-deformed NW sector marked by EW trends. The nature of the interaction (coeval deformation or overprinting) between the two trends is presently unclear, given the kinematically complex zone where these two zones intersect. At the outcrop scale, the JPSZ consists of narrow (10–100 m), subvertical, mylonitic zones with subhorizontal lineations that crosscut all preexisting rock fabrics. Rock foliations parallel to these mylonitic shear zones can be traced into the neighboring country rocks for variable distances ranging from kilometers in the NNW-trending portion in the southeast (fig. 2*a*) to centimeters in the E-W-trending portion of the network in the northwest (fig. 2*b*), suggesting a strain gradient that tapers off to the NW. Mylonitic fabrics are superimposed on a quartzofeldspathic matrix, resulting in asymmetric porphyroclasts (both σ and δ types), the generation of drag folds, and S-C and C-C′ fabrics that consistently record a sinistral sense of shear (fig. 2*a*, 2*b*). Deformation associated with the JPSZ has affected an area up to 200 km wide. This deformation is highly heterogeneous, marked by mylonitic zones with clearly asymmetric fabrics interspersed with less-deformed blocks that are marked by weaker, more symmetric fabrics (fig. 2*c*). On a regional level, the blocks in the SE portion of the JPSZ between the NNW-trending mylonitic zones have a sigmoidal, strike-slip duplex geometry within the larger shear zone structure (fig. 1). This work is based entirely on work in the SE portion where NNW trends predominate.

Feldspar Thermometry

Because the dominant lithology of the Amazon basement is a quartzofeldspathic granitoid, foliations commonly are formed through the deformation of feldspar and quartz. There is a correspondence between the degree of foliation development at the outcrop scale and microstructural textures at the microscopic scale, both of which reflect the degree of strain suffered. K-feldspar grains are characterized by exsolution textures (fig. 3*a*) that range from perthitic grains (lamellae >10 μm) with idiomorphic habits in undeformed igneous rocks in the center of duplex

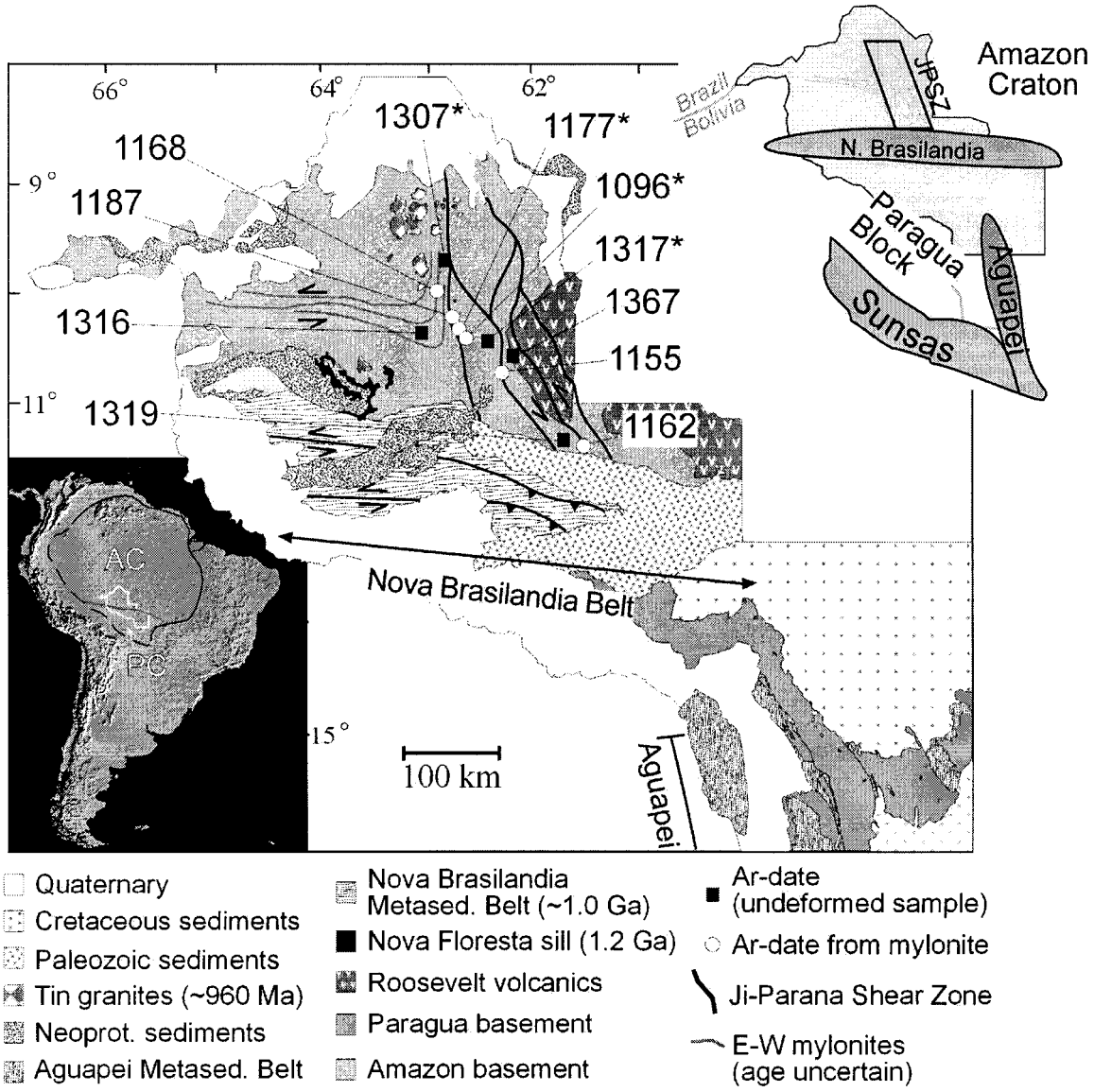

Figure 1. *Bottom inset*, Location map of study area within South American continent, showing relation to general outline of Amazon craton outlined in black. The E-W trace of the Nova Brasilândia belt, a late Mesoproterozoic suture line between the Amazon craton (*AC*) and Paragua craton (*PC*), is shown as a dark gray line. *Top inset*, General geometry of SW Amazon craton showing the deformed basement rocks of Ji-Parana shear zone (JPSZ) with respect to younger (ca. 1.1–1.0 Ga) Nova Brasilândia, Aguapeí, and Sunsas belts. Main location map in Rondônia shows regional trend and large-scale duplex geometry of the NNW-trending JPSZ network superimposed on a simplified geological map adapted from work by Scandolâra et al. (1999); E-trending shear zones, depicted with gray lines, are of uncertain age in relation to JPSZ. $^{40}Ar/^{39}Ar$ ages from hornblende are shown for samples in shear zones and within the undeformed blocks of JPSZ. Numbers are argon plateau ages (total gas ages denoted with asterisks).

blocks and augen gneisses with foliations discordant to the regional trend. Microperthitic feldspars (lamellae <10 μm) are found in banded gneisses with foliations that are parallel to the shear zone boundaries. Coexisting plagioclase grains, preserving rare antiperthitic textures, are found in both undeformed and deformed rocks (e.g., Kroll et al. 1993). A clear correlation exists between the coarseness of the exsolved lamellae in each sample and the overall degree of foliation development resulting from deformation. In contrast with the exsolved textures that characterize weakly foliated granitoids and au-

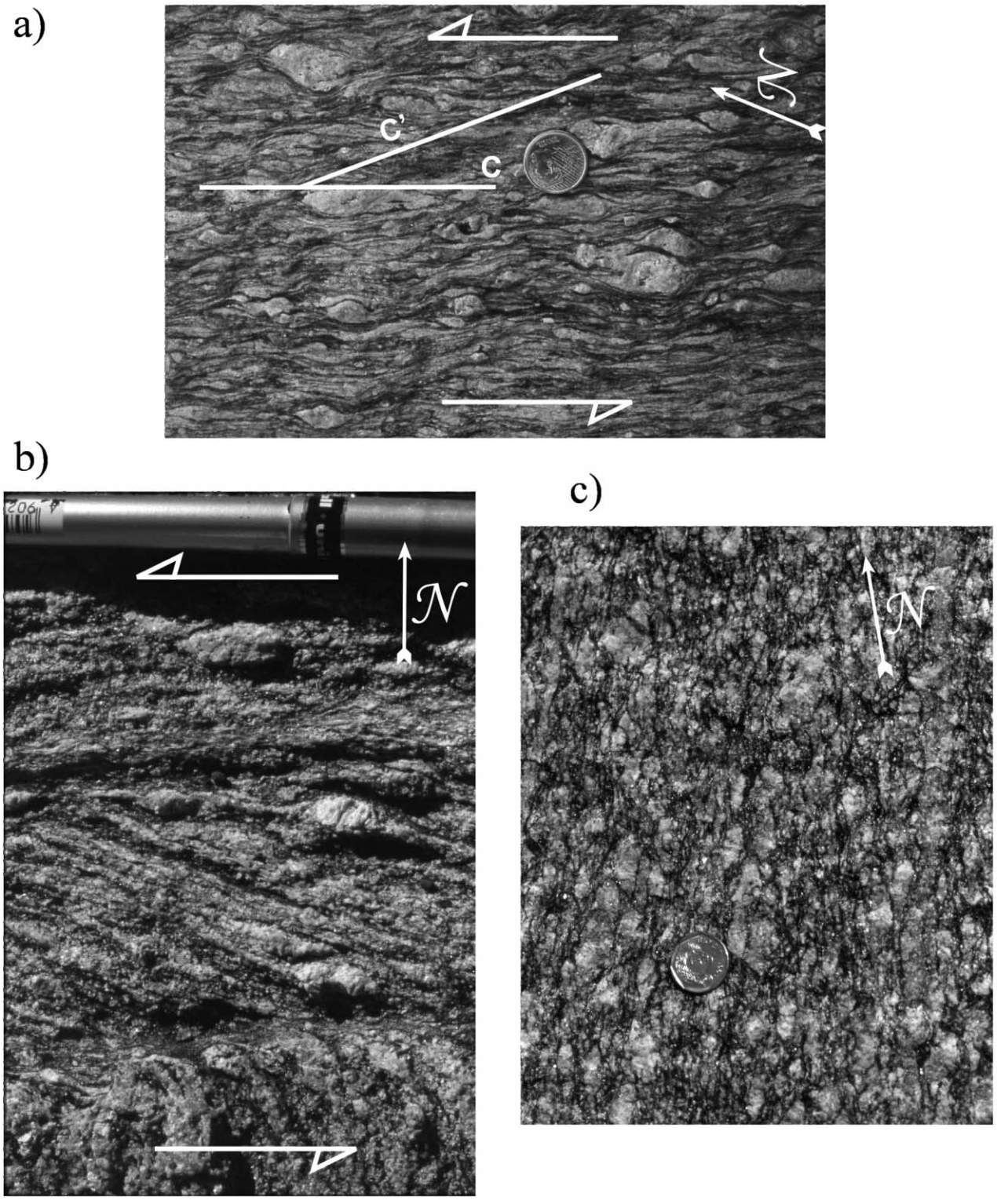

Figure 2. Outcrop photographs looking down at Rondônia basement rocks with north indicated by arrow. *a*, Outcrop photograph of protomylonite from Ji-Parana shear zone. Small drag folds (*below coin*) and C-C′ fabric indicate a sinistral shear sense. Coin on outcrop face is ca. 2.5 cm in diameter. *b*, Outcrop photograph showing the development of sinistral sense shear zone that crosscuts previous rock fabric in NW portion of state, where EW trends predominate. *c*, Weakly developed rock fabric from less deformed interior of shear zone duplex.

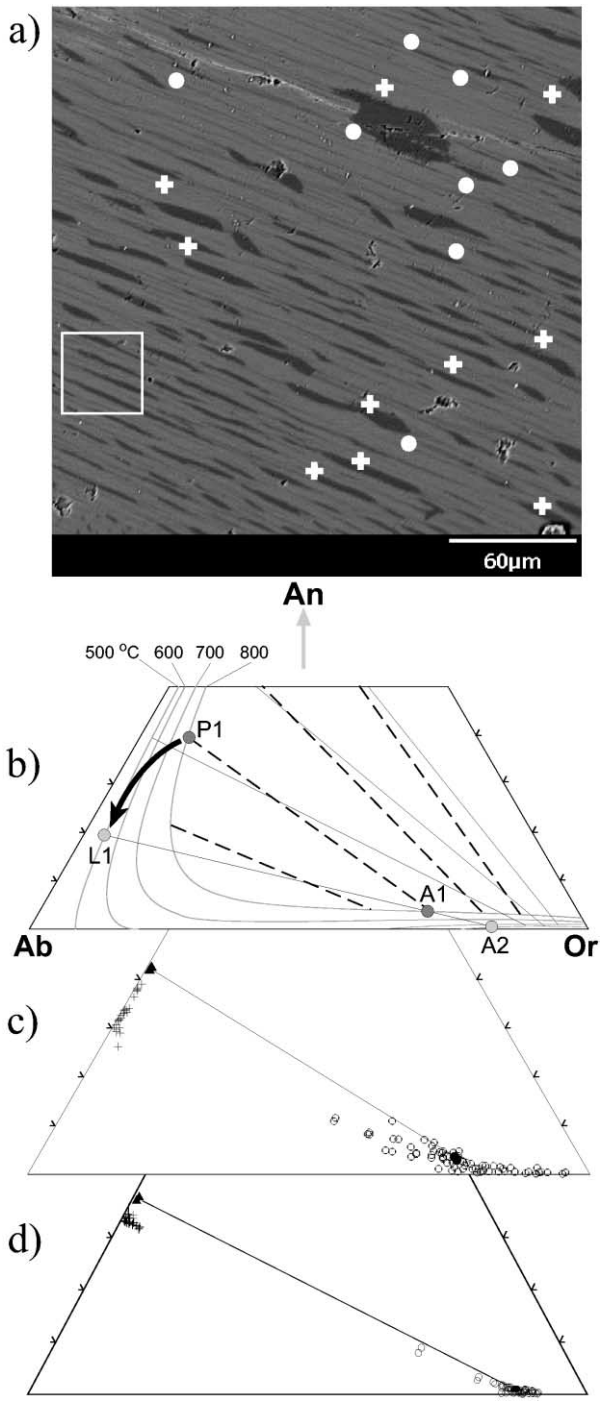

Figure 3. *a*, Backscattered electron image of typical perthitic alkali feldspar grain with schematic representation of analytical procedures. Rectangle depicts open-beam analyses whereas circles and crosses represent typical point analyses. *b*, Feldspar ternary diagram with isothermal solvus locations for 600 MPa plotted from work by Lindsley and Nekvasil (1989) based on *P* estimates in work by Payolla et al. (2002). Curved arrow shows the evolution of lamellar compositions through exsolution in a cooling, static regime. Compositions A1 and P1 are in equilibrium with each other, but cooling to 500°C causes the exsolution of lamellae of composition L1 and drives the host composition to A2. *c*, Representative analyses from a perthitic feldspar grain in an undeformed rock demonstrating migration of lamellar compositions (*crosses*) far from the tie-line connecting reintegrated, original compositions (*open circles* = point analyses of exsolved host K-feldspar; *solid circles* = compositions from reintegration of point analyses of K-feldspar; *filled triangles* = coexistingplagioclase feldspar). *d*, Representative analyses for a banded gneiss sample outside shear zone. Microperthitic feldspar textures indicate that a shorter cooling history after deformation has curtailed the migratory effect of exsolution processes on lamellar compositions.

gen gneisses with foliations discordant to regional trends, shear zone rocks are characterized by the development of a fine-grained, recrystallized matrix of homogeneous feldspar grains. Porphyroclastic feldspars in these mylonitic and protomylonitic samples are characterized by a core-and-mantle structure, with exsolution textures preserved only within the interior of relict clasts. The well-developed 120° triple-point grain boundaries in the mantling grains suggest an equilibrium texture generated by dynamic recrystallization. In deformed samples, the foliation is formed partially by newly formed biotite and hornblende.

Feldspar solvus thermometry can be used to determine the temperature at which coexisting pairs of plagioclase and K-feldspar were in equilibrium (Bohlen and Essene 1977). By assuming that the mineral pairs were in equilibrium at their formation, the compositions of the coexisting pairs can be used to locate the feldspar solvus and thus reconstruct the temperature aspect of the regional cooling (temperature-time) history. In general, temperatures recovered in this way will reflect one of three scenarios: (1) the original igneous emplacement, (2) static recrystallization during metamorphism, or (3) strain-induced recrystallization during deformation. The essential difference among these three cases lies in the principal role of thermal energy for the first two scenarios versus strain energy for the third scenario. Deformation enhances the homogenization and reequilibration of feldspar pairs through subgrain development, recrystallization, and the migration of lamellae out of the host grain (granulation). Thus, textural evidence is critical to determining the significance of the temperature calculations derived from feldspar compositions.

In a slowly cooling terrain undergoing no deformation (case 1), feldspar pairs maintain equilibrium across a widening solvus through mutual exsolution. The uninterrupted growth of exsolution lamellae in K-feldspar results in coarse, perthitic textures (Kroll et al. 1993; Voll et al. 1994). Under these conditions, reintegration of exsolved, unrecrystallized feldspar pairs should recover the original, igneous compositions, thus determining the temperature of emplacement. In the case where recrystallization occurs after emplacement (cases 2 and 3), rock textures provide information regarding the deformation/cooling history. In the case where $T_{\text{recrystallization}} = T_{\text{metamorphism}}$, continued cooling after recrystallization results in the exsolution, producing a microperthitic feldspar texture within a polygonal, unfoliated fabric (case 2) or a foliated, strain-induced fabric (case 3). Where exsolution has taken place, the temperature of recrystallization can be determined from the original compositions at equilibrium prior to exsolution, discussed in "Results." In the case where minimal cooling occurs after deformation (i.e., $T_{\text{metamorphism}} > T_{\text{recrystallization}}$), newly formed grains in the rock foliation will retain a homogeneous composition with no exsolution development. In this scenario, the compositions of the coexisting feldspar pairs are unchanged and directly reflect the temperature of equilibration through recrystallization.

Results

Reintegrated feldspar compositions are given in table 1 with examples of analytical results from single samples (fig. 3) and reintegrated results from all samples (fig. 4) plotted on feldspar ternary diagrams. Two reintegration techniques based on electron microprobe analyses are described in appendix A in the online edition of the *Journal of Geology* and also available from the Data Depository in the *Journal of Geology* office upon request. In general, compositional differences between host and lamella compositions show a clear variance with rock texture. The schematic diagram in figure 3*b* illustrates the general case where protracted cooling leads to extensive exsolution and the development of multiple generations of lamellae, consequently leading to a wide range of lamellar compositions. This general case applies to undeformed to weakly foliated samples with coarse perthitic textures (fig. 3*c*), where the wide range in lamellar compositions off the tie line connecting the coexisting, reintegrated feldspar compositions suggests extended cooling under static conditions (fig. 3*c*). Less-deformed samples tend to record the most highly discordant temperatures, generally with $T_{\text{An}} \gg T_{\text{Or}} > T_{\text{Ab}}$. Samples with gneissic foliation and microperthitic textures have lamellar compositions that plot in a discrete area closer to the K-feldspar–plagioclase tie line (fig. 3*d*), probably reflecting the relatively short duration of time after recrystallization over which exsolution and intercrystalline exchange processes were active. In addition, these gneissic samples record temperatures with a lower degree of discordance between the three thermometers (typically $T_{\text{An}} > T_{\text{Or}} \geq T_{\text{Ab}}$) than that recorded by igneous-textured, coarsely perthitic samples. Reintegrated compositions from all samples are plotted in figure 4. Feldspar pairs from perthitic samples (i.e., both gneissic and igneous) give temperatures in the range of 650°–800°C (fig. 4). In contrast, homogeneous grains from recrystallized mantles in protomylonites and the matrix of mylonitic samples record the lowest temperatures (450°–550°C) with good agreement among the three thermometers ($T_{\text{An}} \approx T_{\text{Or}} \approx T_{\text{Ab}}$).

$^{40}Ar/^{39}Ar$ Geochronology

Hornblende grains were separated from 11 Amazon basement samples (both shear zones and the interior of duplex blocks) for argon isotope analysis. A table with outcrop descriptions, mineral assemblages, and GPS locations is included in appendix form, together with argon isotope data from each sample, and a description of argon analytical techniques (app. B in the online edition of the *Journal of Geology* and also available from the Data Depository in the *Journal of Geology* office upon request). Two sets of hornblende ages are observed, an older set of clustering at ca. 1.35 Ga and a younger set of ages in the 1.18–1.15-Ga range (fig. 1). A close correspondence is observed between the $^{40}Ar/^{39}Ar$ ages and the structural setting of the sample. Samples from the duplex interiors record older ages, similar to ages preserved in U-Pb analysis of monazite as well as those from garnet–whole rock Sm-Nd isochrons from rocks to the north of this study area (Payolla et al. 2002; Tohver et al. 2005). Mylonitic samples invariably record argon ages that are reset to the 1.18–1.15-Ga range. The different age ranges correspond to the feldspar thermometry results, with samples that yield temperatures >600°C, preserving ages in the older 1.35-Ga range. In contrast, reset ages in the 1.18–1.15-Ga range are found in mylonitic and protomylonitic shear zone samples, where feldspar thermometry records temperatures in the 450°–550°C range. The younger set of hornblende ages are regarded as marking the timing of deformation-induced recrystallization be-

Table 1. Electron Microprobe Analyses for Reintegrated Feldspar Compositions and Thermometry Data

	103★		107★		109★		110★		112★		113★		117★		120★	
Sample	Plag	Kspar	Plag	Kspar	Plag	Kspar	Plag	Kspar	Plag	Kspar	Plag	Kspar	Plag	Kspar	Plag	Kspar
Na_2O	8.41	1.10	8.31	2.60	7.19	1.56	8.35	2.31	8.16	2.02	7.87	1.91	9.61	3.12	7.68	1.60
CaO	5.69	.12	5.57	.62	7.42	.36	5.83	.50	5.84	.30	6.57	.33	3.66	.35	6.89	.16
K_2O	.18	14.85	.20	12.84	.17	14.25	.16	13.25	.45	13.76	.44	13.85	.20	12.19	.22	14.41
Al_2O_3	24.45	18.67	24.57	19.56	26.36	19.32	24.69	19.47	24.09	18.61	25.33	19.15	22.95	19.34	25.90	19.09
SiO_2	61.40	64.56	60.63	63.89	57.96	63.93	59.45	62.70	59.99	63.75	58.65	64.66	64.00	64.85	60.15	64.29
Fe_2O_3	.02	.05	.05	.01	.05	.02	.07	.13	.34	.08	.08	.04	.07	.10	.07	.11
Total	100.15	99.34	99.34	99.52	99.16	99.44	98.56	98.36	98.87	98.52	98.93	99.94	100.48	99.95	100.91	99.65
Na	.722	.098	.720	.229	.627	.139	.728	.207	.711	.182	.685	.169	.818	.274	.657	.142
Ca	.270	.006	.266	.030	.358	.017	.281	.024	.281	.015	.316	.016	.172	.017	.326	.008
K	.010	.880	.011	.758	.010	.842	.009	.788	.027	.818	.025	.811	.011	.714	.012	.847
Al	1.277	1.020	1.293	1.059	1.397	1.052	1.308	1.067	1.276	1.020	1.339	1.035	1.187	1.041	1.347	1.037
Si	2.720	2.995	2.708	2.939	2.607	2.955	2.672	2.916	2.696	2.968	2.632	2.967	2.809	2.962	2.655	2.962
Fe	.001	.002	.002	.000	.002	.001	.002	.005	.011	.003	.003	.001	.002	.003	.002	.004
X (An)	27.0	.6	26.7	3.0	36.0	1.7	27.6	2.4	27.6	1.4	30.8	1.5	17.2	1.7	32.7	.8
X (Ab)	72.0	10.0	72.1	22.7	63.0	13.9	71.5	20.3	69.8	17.9	66.8	17.0	81.7	27.4	66.0	14.3
X (Or)	1.0	89.5	1.2	74.6	1.0	84.5	.9	77.4	2.6	80.7	2.5	81.5	1.1	71.1	1.2	84.9
Unadjusted:																
T(Ab)	486		637		573		622		620		618		647		583	
T(Or)	462		488		494		464		579		586		448		502	
T(An)	618		940		762		873		725		745		834		605	
Na-K adjusted:																
T(Ab)	576		677		631		661		673		683		680		599	
T(Or)	576		608		631		600		668		680		568		599	
T(An)	576		899		733		840		689		703		786		599	

	123★		122 r		104 r		105 r		110 r		113 r		115 r		125 r	
	Plag	Kspar	Plag	Kspar	Plag	Kspar	Plag	Kspar	Plag	Kspar	Plag	Kspar	Plag	Kspar	Plag	Kspar
Na_2O	7.14	2.28	8.30	1.30	8.64	1.18	8.41	.67	8.60	1.09	7.68	1.37	8.79	.93	10.03	.44
CaO	7.45	.27	5.49	.09	5.48	.01	5.40	.03	5.42	.01	6.89	.12	4.88	.01	2.78	.00
K_2O	.35	13.23	.57	13.76	.12	15.08	.16	15.32	.11	15.35	.19	14.59	.17	15.28	.50	17.00
Al_2O_3	26.02	18.94	24.35	18.62	24.02	18.52	23.87	18.25	23.85	18.43	25.76	19.02	23.30	18.03	21.91	18.40
SiO_2	58.58	63.98	62.62	64.30	61.91	64.30	61.16	65.16	61.80	64.54	59.62	65.10	62.03	64.73	65.99	64.36
Fe_2O_3	.14	.13	.09	.05	.13	.02	.10	.08	.01	.12	.06	.04	.05	.04	.02	.03
Total	99.68	98.83	101.43	98.11	100.30	99.11	99.1058	99.51	99.79	99.54	100.21	100.25	99.23	99.01	101.21	100.23
Na	.620	.204	.715	.117	.740	.11	.730	.06	.74	.10	.661	.122	.761	.08	.85	.04
Ca	.358	.013	.262	.004	.260	.001	.259	.001	.258	.001	.328	.006	.233	.001	.26	.00
K	.020	.784	.033	.826	.007	.894	.009	.908	.006	.906	.011	.855	.009	.908	.03	1.00
Al	1.374	1.034	1.277	1.031	1.251	1.013	1.259	.999	1.249	1.005	1.349	1.028	1.226	.990	1.12	1.00
Si	2.624	2.965	2.788	3.022	2.737	2.986	2.74	3.028	2.746	2.987	2.649	2.987	2.769	3.016	2.87	2.96
Fe	.005	.005	.003	.002	.00	.001	.00332	.003	.000	.004	.002	.002	.00	.001	.00	.00
X (An)	35.9	1.3	26.3	.4	25.8	.1	25.9	.1	25.7	.1	32.8	.6	23.3	.1	22.7	.0
X (Ab)	62.1	20.3	71.8	12.3	73.5	10.6	73.1	6.2	73.7	9.7	66.1	12.4	75.8	8.5	74.6	3.8
X (Or)	2.0	78.4	3.5	87.3	.7	89.4	.9	93.6	.6	90.2	1.1	87.0	.9	91.4	2.7	96.2
Unadjusted:																
T(Ab)	676		553		468		452		453		551		424		397	
T(Or)	577		553		369		456		374		491		388		398	
T(An)	646		553		369		456		374		568		388		398	
Na-K adjusted:																
T(Ab)	659		553		523		455		509		563		396		398	
T(Or)	659		553		498		455		492		563		396		398	
T(An)	659		553		349		455		355		563		396		398	

Note. Electron microprobe data and mineral formulas values are given, prior to adjustment for K-Na exchange. Asterisk = a reintegrated feldspar pair; r = a recrystallized, homogeneous sample; Kspar = K-feldspar; Plag = plagioclase.

cause the deformation temperatures determined from feldspar thermometry of these shear zones are similar to the hornblende blocking temperature of radiogenic argon (Harrison 1981).

Despite the clear correspondence of the structural setting of the samples, the results of feldspar thermometry, and the $^{40}Ar/^{39}Ar$ ages, there are some difficulties inherent in the dating of deformation. The error estimates for the feldspar thermometer are accentuated by the steepness of the solvus limbs at low temperatures. In addition, given the uncertainty of assigning a single blocking temperature for hornblende, it is difficult to determine whether these younger ages represent the exact timing of deformation or minor cooling from deformation, where $T_{\text{deformation}} \approx T_{\text{blocking}}$. Regardless, the preservation of older ages in the duplex interior indicates that regional metamorphic conditions during the shearing event were not sufficiently high to thermally reset hornblende grains without dynamic processes beginning at ca. 1.18 Ga.

Discussion

The SW Amazon craton was affected by widespread deformation during the 1.18–1.15-Ga interval. This deformation was accommodated by a network of sinistral, strike-slip shear zones referred to collectively as the Ji-Paraná shear zone. The predominantly strike-slip nature of these shear zones is inferred from their nearly vertical attitude with low rake mineral lineations and especially by shear sense indicator orientations. Results from feldspar thermometry reveal that shear zone activity occurred at temperatures of 450°–550°C, with higher temperatures (>600°C) recovered from the less-deformed to undeformed interiors of duplex blocks. The deformation-induced recrystallization in mylonitic shear zones was responsible for age resetting, a conclusion further supported by the preservation of older ages, ca. 1.35 Ga, in the interior of duplex blocks. Thus, the wide range in ages recorded by $^{40}Ar/^{39}Ar$ analysis of hornblende can be attributed to episodic activation of individual shear zones and not to differences in cooling rate among different crustal domains. The strike-slip environment appears not to have resulted in significant crustal thickening, which would have produced uniform isotopic age resetting related to the relaxation of crustal isotherms. Kinematic indicators from individual mylonitic shear zones indicate sinistral offsets throughout the JPSZ network, although a full understanding of the overall kinematic framework awaits future studies that identify the full extent of this deformation episode (e.g., the EW-trending shear zones to the NW of this study area). One factor that complicates this task is the possibility that portions of the Amazon craton may have been stranded as exotic terranes during Grenvillian tectonism, leaving incomplete the kinematic framework of the SW Amazon craton (e.g., Carrigan et al. 2003; Loewy et al. 2003; Tohver et al. 2004*a*).

The continent-continent collision that marks the beginning of a common geological history for Laurentia and Amazonia (fig. 5) is based on paleomagnetic data for both continents at ca. 1.2 Ga (Tohver et al. 2002). Because this collision is the starting point of the search for a compatible metamorphic history, any overlap in ages of geological events on both cratons for times before 1.2 Ga is unrelated to a common paleogeography. For southern Laurentia, the limit of Grenvillian deformation is the NE-SW-trending Llano Front (Denison et al. 1984), a prominent magnetic and gravity anomaly. Originally proposed as the boundary between cratonic elements with Nd model ages greater than 1.55 Ga and accreted arcs with Nd model ages less than 1.55 Ga and U-Pb ages of ca. 1.35 Ga (Van Schmus et al. 1996; Mosher 1998), the isotopic significance of the Llano Front has been called into question by recent work of Barnes et al. (1999), who demonstrated that older, ca. 1.7-Ga Laurentian crust is present to the south of the boundary as presently drawn. Regardless, the Llano Front separates the undeformed, stable craton to the NW from rocks affected by Grenvillian deformation to the SE (Mosher 1998). The timing of the accretion of the juvenile, 1.35-Ga Coal Creek volcanic arc south of this boundary is uncertain (Roback 1996). Mosher (1998) pointed to abundant felsic magmatism at 1.25 Ga as possibly related to the docking of the Coal Creek volcanic arc but favors another model with simultaneous accretion of the island arc during the later episode of continent-continent collision that was chiefly responsible for regional deformation and metamorphism. Support for this second, preferred model is found in observations of bimodal volcanism in west Texas beginning as early as 1.25 Ga, interpreted to reflect an extensional tectonic environment (Bickford et al. 2000). If so, these observations are at odds with the collisional environment required by the "early" 1.25-Ga arc accretion model.

Constraints on the timing of the major collisional event itself are established by the dating of pretectonic and posttectonic sills and dikes, bracketed between $1238 + 8/-6$ and $1098 + 3/-2$ Ma (Walker 1992). In addition, the dating of metamorphic zircon (1147 ± 2 Ma, 1128 ± 6 Ma) from eclo-

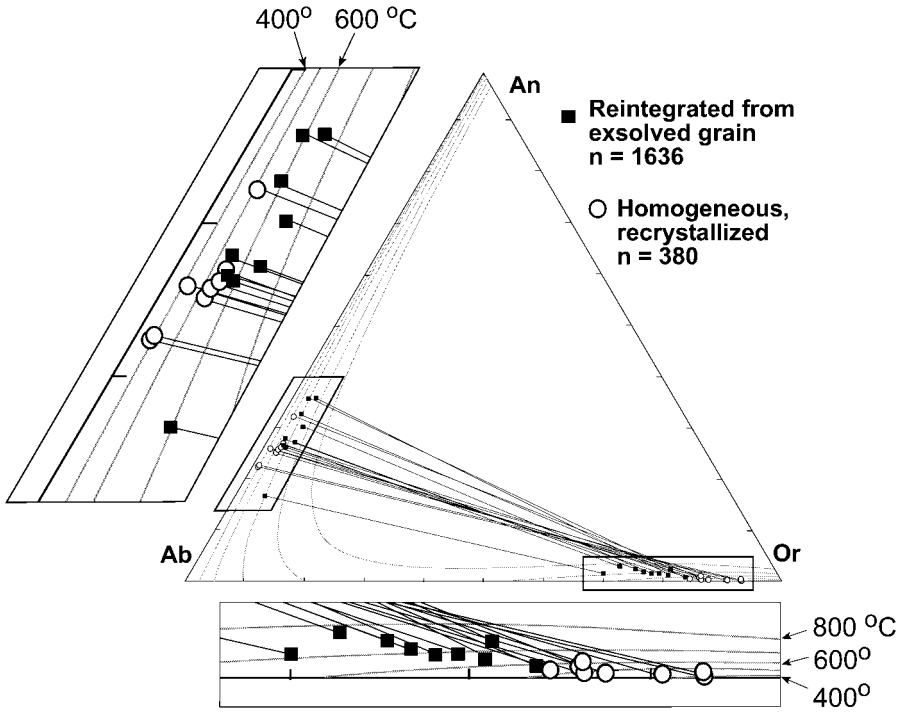

Figure 4. Summary plot of 17 samples with coexisting reintegrated feldspar compositions corrected for late-stage K-Na exchange, with enlargements at left and bottom to illustrate relation of reintegrated compositions to solvi. Squares indicate reintegrated compositions from samples with perthitic textures, and circles indicate compositions from homogeneous, recrystallized grains.

gitic rocks provides a minimum age of Llano tectonic activity (Roback and Carlson 1996) The collision resulted in substantial crustal thickening through both subduction and thrust faulting. Eclogites are reported as having equilibrated at pressures of >1.5 GPa at 500°C, while more regionally extensive gneisses record pressures of 800 MPa and temperatures of ~750°C (Wilkerson et al. 1988; Carlson and Schwarze 1997). This phase of active deformation, ascribed to A-type subduction, is considered to have ceased by 1098 Ma, a time marked by the extensive emplacement of postorogenic granites, resulting in widespread age resetting of the $^{40}Ar/^{39}Ar$ and Rb-Sr systems (Wilkerson et al. 1988; Rougvie et al. 1999). The upper age limit on low-grade deformation in west Texas was established by the discovery of ca. 1.12-Ga zircons reported by Roths (1993) from granitic clasts in deformed, conglomeratic sediments overlying the >1.24-Ga basement (Bickford et al. 2000). Bickford and others (2000) reported $^{40}Ar/^{39}Ar$ ages of 1.04 Ga for both hornblende and muscovite from shear zones, interpreted as the deformation age. New $^{40}Ar/^{39}Ar$ data reported by Grimes and Copeland (2004) extends the range of this late deformation episode to between 1.02 and 1.06 Ga. Thus, the greenschist/lower amphibolite deformation observed in west Texas is considerably (100–150 Ma) younger than the major, high-grade collisional event affecting the Llano Uplift (fig. 5).

Major deformation of the Llano region during the collisional phase of orogeny was marked by the formation of multiple generations of noncoaxial folds, with fivefold generations verging generally to the NE (Mosher 1998). Asymmetric fabrics in mylonitic shear zones also indicate general tectonic transport direction to the NE (Carter 1989; Mosher 1998; Reese and Mosher 2004), that is, nearly parallel to the Llano Front itself, which is indicative of bulk motion in an oblique collision zone (Carter 1989). Recent structural work in the Llano region confirms the NE trend of tectonic transport, ascribed to the docking of a continent to the south (Reese and Mosher 2004). Similar overprinting relationships of successive fold generations during earlier high-grade deformation of the west Texas basement was interpreted to reflect sinistral, strike-slip displacement by Bristol and Mosher (1989), presumably after an early 1.25-Ga extensional phase reported by Bickford et al. (2000). Deformation un-

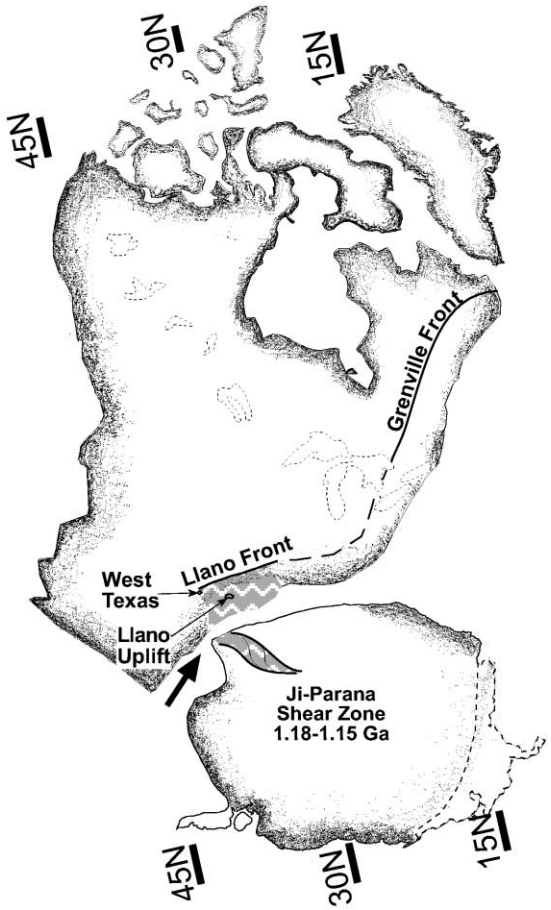

Figure 5. Paleogeographic reconstruction of the oblique collision between southern Laurentia and the Amazon craton based on paleomagnetic data (modified from Tohver et al. 2002). Orthogonal map projection of Laurentia (in modern orientation) is centered on 30° of the ca. 1.2-Ga coordinates. Large arrow shows tectonic transport direction inferred for the Llano region by Mosher (1998). The inferred subsurface connection between the Grenville Front and Llano Front is shown as a dashed line in the midcontinental United States.

der low-grade conditions affected the southern Laurentian margin long after the main collisional event was over; strike-slip zone bounded basins in west Texas exposures interpreted as transpressional (Soegaard and Callahan 1994) were active approximately 100–150 Ma after the main deformational episode affected the Llano Uplift region (Bickford et al. 2000). The dextral offset observed during this later episode of deformation contrasts with the earlier sinistral motion, possibly reflecting either a change in relative plate motions, as proposed by Grimes and Mosher (2003), or a change in localized stress fields from continuous (ca. 100–150 Ma) indentor tectonics, as originally suggested by Mosher (1998).

A comparison of the Grenville history recorded in the SW Amazon craton with that observed in southernmost Laurentia reveals overlap in the ages of tectonic activity (fig. 6), with most Amazon ages in the 1.18–1.15-Ga range and Llano ages in the 1.15–1.10-Ga range. One possible explanation for the older ages preserved in the Amazon lies in the style of deformation recorded in both continents. The deformation registered in the Amazon craton is marked chiefly by strike-slip faults that caused minimal crustal thickening during the early Grenville (ca. 1.18–1.15 Ga) episode. The preservation of an earlier, ca. 1.35-Ga metamorphic history by the $^{40}Ar/^{39}Ar$ system in hornblende outside of shear zones is evidence of a lack of thermal resetting following crustal thickening. The development of strike-slip faults rather than thrust faults signals a different geological meaning for Grenvillian (1.18–1.15 Ga) age data reported here from the SW Amazon craton, compared with slightly younger Grenvillian (1.15–1.10 Ga) ages from southern Laurentia. Namely, Amazon hornblende ages from shear zones record the timing of deformation, not the age of cooling through the hornblende blocking temperature. In contrast, substantial crustal thickening and resultant heating in the Llano region mean that only minerals with higher blocking temperatures, such as zircon or monazite have the potential to record the early orogenic history. Given the clockwise *PT* loop expected for continent-continent collision, the peak thermal conditions will postdate the high *P*–low *T* conditions that mark the onset of the collision itself. This fact aside, the inference that Llano region age data from metamorphic minerals provide a minimum age constraint for the timing of collision-related deformation is supported by numerous U-Pb studies of high-pressure terranes that conclude that metamorphic zircon is more likely to grow during the retrograde portion of the *PT* path, that is, during the postcollisional exhumation phase (e.g., Roberts and Finger 1997; Fernandez-Suarez et al. 2002; Whitehouse and Platt 2003; Timmerman et al. 2004). Like the Ontario–New York segment of the Grenville Province (e.g., Mezger et al. 1993) geochronological constraints on tectonism in southern Laurentia established by dating of metamorphic minerals probably reflect the postcollisional phase of orogenesis, not the timing of deformation itself, as is the case with the SW Amazon craton.

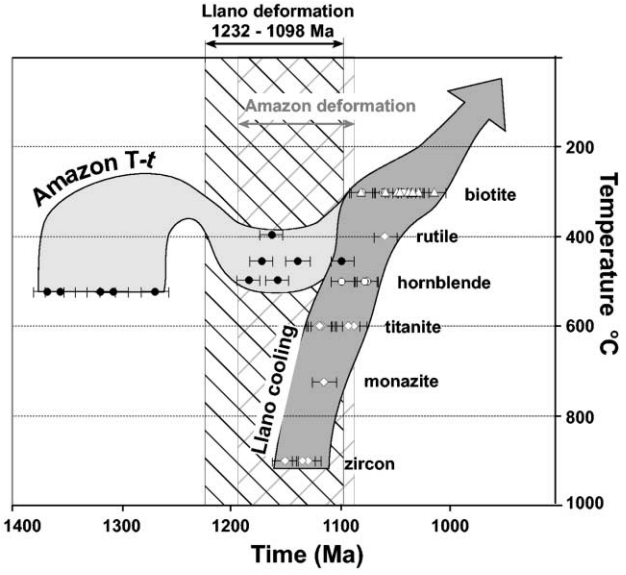

Figure 6. Comparison of the time-temperature evolution of the Llano province (*white symbols*) and the deformation ages reported here for the SW Amazon craton (*black symbols*). U-Pb data are represented by diamonds, ^{40}Ar-^{39}Ar data are shown as circles, and Rb-Sr data are shown as diamonds. The black crosshatched area shows the absolute constraints on the timing of Llano deformation (1.24–1.10 Ga) reported by Walker (1992) and Mosher (1998). Llano geochronological data are compiled from work by Reese et al. (1996), Mosher (1998), and Rougvie et al. (1999), which we interpret as reflecting cooling postdating deformation of a crustally thickened orogenic zone. Amazon ages in the 1.18–1.15 Ga range from ^{40}Ar/^{39}Ar analysis of hornblende are interpreted as recording deformation ages related to collision with southern Laurentia. The range in ages for this deformation is shown by gray crosshatching in the region that overlaps absolute constraints on Llano region deformation. The variation in temperature assigned to these ages is based on temperatures of deformation determined from feldspar thermometry. Older, ca. 1.35-Ga ages are depicted as recording cooling through the hornblende blocking temperature from an older high-grade event.

Conclusions

The SW margin of the Amazon craton is marked by a wide network of shear zones (~200 km), called the Ji-Paraná shear zone, which is characterized by sinistral strike-slip displacement. The ^{40}Ar/^{39}Ar age data and feldspar thermometry reveal at least two metamorphic episodes that affected the Amazon basement rocks. Vestiges of an older event at ca. 1.35 Ga are observed in widespread gneissic fabrics that reflect strain under upper amphibolitic to granulitic conditions. Displacement along the JPSZ took place at upper greenschist/lower amphibolite conditions that reset argon ages. The timing of this deformation varies from ca. 1.18 to 1.15 Ga, which is compatible with the broad limits of Grenvillian deformation in southern Laurentia. We interpret the difference between deformation ages preserved in Amazonia and the somewhat younger ages of southern Laurentia (cooling/retrograde growth ages) as a natural consequence of the clockwise *PT* loop expected for collision tectonics. This difference in the geological significance of geochronological data underlies the compatibility of the tectonometamorphic histories preserved on both sides of the collisional orogen. The inferred asymmetrical orogenic structure is supported by observations of widespread crustal thickening in Laurentia accommodated by thrust faults, contrasted with the predominantly strike-slip deformation of the SW Amazon craton. These observations expand on the previously proposed collision between the SW Amazon craton and southernmost Laurentia during early Grenvillian times (ca. 1.2 Ga). Further work is necessary to understand fully the kinematics of the interactions between Amazonia and Laurentia and its implications for Rodinia reconstructions.

ACKNOWLEDGMENTS

Fieldwork was supported with assistance from the Stichting Shurmannfonds to B. van der Pluijm. We thank R. da Silva Sousa and the Companhia de Pesquisa de Recursos Minerais office of Porto Velho for the generous support of fieldwork in Rondônia. Laboratory work was funded by National Science Foundation (NSF) grant EAR-02-30059 and the Scott Turner Fund of the University of Michigan. We thank M. Johnson and C. Hall for assistance at the University of Michigan argon geochronology laboratory and C. Henderson for help with the electron microprobe in the R. B. Mitchell Electron Microbeam Laboratory, which was funded in part by NSF grants EAR 99-11352 and EAR 96-28196. Helpful reviews by S. Mosher, M. E. Bickford, and E. Hartz significantly improved the manuscript.

REFERENCES CITED

Barnes, M. A.; Rohs, C. R.; Anthony, E. Y.; Van Schmus, W. R.; and Dension, R. E. 1999. Isotopic and elemental chemistry of subsurface Precambrian igneous rocks, west Texas and eastern New Mexico. Rocky Mt. Geol. 34:245–262.

Bettencourt, J. S.; Tosdal, R. M.; Leite, W. B.; and Payolla, B. L. 1999. Mesoproterozoic rapakivi granites of the Rondônia Tin Province, southwestern border of the Amazonian craton, Brazil. I. Reconnaissance U-Pb geochronology and regional implications. Precambrian Res. 95:41–67.

Bickford, M. E.; Soegaard, K.; Nielsen, K. C.; and McLelland, J. M. 2000. Geology and geochronology of Grenville-aged rocks in the Van Horn and Franklin Mountains area, west Texas: implications for the tectonic evolution of Laurentia during the Grenville. Geol. Soc. Am. Bull. 112:1134–1148.

Bohlen, S. R., and Essene, E. J. 1977. Feldspar and oxide thermometry of granulites in the Adirondack Highlands. Contrib. Mineral. Petrol. 62:153–169.

Bristol, D. A., and Mosher, S. 1989. Grenville-age, polyphase deformation of mid-Proterozoic basement, NW Van Horn Mountains, Trans-Pecos, Texas. J. Geol. 97: 25–43.

Carlson, W., and Schwarze, E. 1997. Petrological significance of prograde homogenization of growth zoning in garnet: an example from the Llano Uplift. J. Metamorph. Geol. 15:631–644.

Carrigan, C. W.; Miller, C. F.; Fullagar, P. D.; Bream, B. R.; Hatcher, R. D.; and Coath, C. D. 2003. Ion microprobe age and geochemistry of southern Appalachian basement, with implications for Proterozoic and Paleozoic reconstructions. Precambrian Res. 120:1–36.

Carter, K. E. 1989. Grenville orogenic affinities in the Red Mountain area, Llano County, Texas. Can. J. Earth Sci. 26:1124–1135.

Cawood, P. A.; McCausland, P. J. A.; and Dunning, G. R. 2001. Opening Iapetus: constraints from the Laurentian margin in Newfoundland. Geol. Soc. Am. Bull. 113:443–453.

Dalziel, I. W. D.; Mosher, S.; and Gahagan, L. M. 2000. Laurentia-Kalahari collision and the assembly of Rodinia. J. Geol. 108:499–513.

Davidson, A. 1998. An overview of the Grenville Province, Canadian Shield. *In* Geology of the Precambrian Superior and Grenville Provinces and Precambrian fossils in North America. Geol. Can. 7:205–270.

Denison, R. E.; Lidiak, E. G.; Bickford, M. E.; and Kisvarsanyi, E. B. 1984. Geology and geochronology of Precambrian rocks in the central interior region of the United States. U.S. Geol. Surv. Prof. Pap. 1241-C, 33 p.

Easton, R. M. 1992. The Grenville Province and the Proterozoic history of central and southern Ontario. Ont. Geol. Surv. Spec. Vol. 4:715–904.

Fernandez-Suarez, J.; Corfu, F.; Arenas, R.; Marcos, A.; Catalan, J. R. M.; Garcia, F. D.; and Abati, J. 2002. U-Pb evidence for a polyorogenic evolution of the HP-HT units of the NW Iberian Massif. Contrib. Mineral. Petrol. 143:236–253.

Fuhrman, M. L., and Lindsley, D. H. 1988. Ternary feldspar modeling and thermometry. Am. Mineral. 73: 201–215.

Gower, C. F.; Ryan, A. B.; and Rivers, T. 1990. Mid-Proterozoic Laurentia-Baltica: an overview of its geological evolution and a summary of the contributions made by this volume. Geol. Assoc. Can. Spec. Pap. 38:1–13.

Grimes, S. W., and Copeland, P. 2004. Thermochronology of the Grenville Orogeny in west Texas. Precambrian Res. 131:23–54.

Grimes, S. W., and Mosher, S. 2003. Structure of the Carrizo Mountain Group, southeastern Carrizo Mountains, west Texas: a transpressional zone of the Grenville orogen. Tectonics 22:1003; doi/10.1029/2001TC001316.

Hanson, R. E.; Crowley, J. L.; Bowring, S. A.; Ramezani, J.; Gose, W. A.; Dalziel, I. W. D.; Pancake, J. A.; Seidel, E. K.; Blenkinsop, T. G.; and Mukwakwami, J. 2004. Coeval large-scale magmatism in the Kalahari and Laurentian cratons during Rodinia assembly. Science 304:1126–1129; doi/10.1126/science.1096329.

Harrison, M. 1981. Diffusion of ^{40}Ar in hornblende. Contrib. Mineral. Petrol. 78:324–331.

Hartz, E. H., and Torsvik, T. H. 2002. Baltica upside down: a new plate tectonic model for Rodinia and the Iapetus Ocean. Geology 30:255–258.

Hoffman, P. F. 1991. Did the breakout of Laurentia turn Gondwana inside out? Science 252:1409–1412.

Jacobs, J.; Bauer, W.; and Fanning, C. M. 2003. New age constraints for Grenville-age metamorphism in western central Dronning Maud Land (East Antarctica), and implications for the palaeogeography of Kalahari in Rodinia. Int. J. Earth Sci. 92:301–315; doi/10.1007/s00531-003-0335-x.

Jacobs, J.; Thomas, R. J.; and Weber, K. 1993. Accretion and indentation tectonics at the southern edge of the Kaapvaal craton during the Kibaran (Grenville) orogeny. Geology 21:203–206.

Kroll, H.; Evangelakakis, C.; and Voll, G. 1993. Two-feldspar thermometry: a review and revision for slowly cooled rocks. Contrib. Mineral. Petrol. 114: 510–518.

Lindsley, D. H., and Nekvasil, H. 1989. A ternary feldspar model for all reasons. EOS: Trans. Am. Geophys. Union 70:506.

Litherland, M.; Annells, R. N.; Darbyshire, D. P. F.; Fletcher, C. J. N.; Hawkins, M. P.; Klinck, B. A.; Mitchell, W. I., et al. 1989. The Proterozoic of eastern Bolivia and its relationship to the Andean mobile belt. Precambrian Res. 43:157–174.

Loewy, S. L.; Connelly, J. N.; Dalziel, I. W. D.; and Gower, C. F. 2003. Eastern Laurentia in Rodinia: constraints from whole rock Pb and U/Pb geochronology. Tectonophysics 375:169–197.

Mezger, K.; Essene, E. J.; van der Pluijm, B. A.; and Halliday, A. N. 1993. U-Pb geochronology of the Grenville Orogen of Ontario and New York: constraints on ancient crustal tectonics. Contrib. Mineral. Petrol. 114: 13–26.

Mosher, S. 1998. Tectonic evolution of the southern Laurentian Grenville orogenic belt. Geol. Soc. Am. Bull. 110:1357–1375.

Payolla, B. L.; Bettencourt, J. S.; Kozuch, M.; Leite, W. B.; Fetter, A. H.; and Van Schmus, W. R. 2002. Geological evolution of the basement rocks in the east-central part of the Rondônia Tin Province, SW Amazon craton, Brazil: U-Pb and Sm-Nd isotopic constraints. Precambrian Res. 119:141–169.

Piper, J. D. A. 1987. Paleomagnetism and the continental crust. New York, Open University Press, 434 p.

Powell, C. M.; Jones, D. L.; Pisarevsky, S.; and Wingate, M. T. D. 2001. Palaeomagnetic constraints on the position of the Kalahari craton in Rodinia. Precambrian Res. 110:33–46; doi/10.1016/S0301-9268(01)00179-6.

Raase, P. 1998. Feldspar thermometry: a valuable tool for deciphering the thermal history of granulite-facies rocks, as illustrated with metapelites from Sri Lanka. Can. Mineral. 36:67–86.

Reese, J. F., and Mosher, S. 2004. Kinematic constraints on Rodinia reconstructions from the core of the Texas Grenville orogen. J. Geol. 112:185–205.

Rivers, T. 1997. Lithotectonic elements of the Grenville Province: review and tectonic implications. Precambrian Res. 86:117–154.

Rivers, T.; Martignole, J.; Gower, C. F.; and Davidson, A. 1989. New tectonic divisions of the Grenville Province, southeast Canadian shield. Tectonics 8:63–84.

Roback, R. C. 1996. Characterization and tectonic evolution of a Mesoproterozoic island arc in the southern Grenville Orogen, Llano uplift, central Texas. Tectonophysics 265:29–52.

Roback, R. C., and Carlson, W. D. 1996. Constraining the timing of high-P metamorphism in the Llano Uplift through geochronology of eclogitic rocks. Geol. Soc. Am. Abstr. Program 28:60–61.

Roberts, M. P., and Finger, F. 1997. Do U-Pb zircon ages from granulites reflect peak metamorphic conditions? Geology 25:319–322.

Roths, P. J. 1993. Geochemical and geochronological studies of the Grenville-age (1250–1000 Ma) Allamoore and Hazel Formations, Hudspeth and Culberson counties, west Texas. *In* Soegaard, K.; Nielsen, K. C.; Marsaglia, K. M.; and Barnes, C. G., eds. Precambrian geology of the Franklin Mountains and Van Horn Area, Trans-Pecos Texas: Dallas, Texas. Geol. Soc. Am. SC Sect. Meeting Guidebook, University of Texas, p. 11–35.

Rougvie, J. R.; Carlson, W. D.; Copeland, P.; and Connelly, J. N. 1999. Late thermal evolution of Proterozoic rocks in the northeastern Llano Uplift, central Texas. Precambrian Res. 94:49–72.

Samson, S. D., and Alexander, E. C. 1987. Calibration of the interlaboratory $^{40}Ar/^{39}$ standard Mmhb-1. Chem. Geol. 66:27–34.

Scandolâra, J. E.; Rizzotto, G. J.; Amorim, J. L.; Bahia, R. B. C.; Quadros, M. L.; and da Silva, C. R. 1999. Geological map of Rondônia, scale 1 : 1,000,000. Rio de Janeiro, Companhia de Pesquisa de Recursos Minerais.

Soegaard, K., and Callahan, D. M. 1994. Late Middle Proterozoic Hazel Formation near Van Horn, Trans-Pecos Texas: evidence for transpressive deformation in Grenvillian basement. Geol. Soc. Am. Bull. 106:413–423.

Tassinari, C. C. G.; Bettencourt, J. S.; Geraldes, M. C.; Macambira, M. J. B.; and Lafon, J. M. 2000. The Amazonian Craton. *In* Tectonic evolution of South America, Int. Geol. Cong., 31st (Rio de Janeiro, 2000), p. 41–97.

Timmermann, H.; Štědra, V.; Gerdes, A.; Noble, S. R.; Parrish, R. R.; and Dörr, W. 2004. The problem of dating high-pressure metamorphism: a U-Pb isotope and geochemical study on eclogites and related rocks of the Mariánské Lázně Complex, Czech Republic. J. Petrol. 45:1311–1338.

Tohver, E.; Bettencourt, J. S.; Tosdal, R.; Mezger, K.; Luiz, W. B.; and Payolla, B. L. 2004*a*. Terrane transfer during the Grenville orogeny: tracing the Amazonian ancestry of southern Appalachian basement through Pb and Nd isotopes. Earth Planet. Sci. Lett. 228:161–176.

Tohver, E.; van der Pluijm, B. A.; Mezger, K.; Essene, E. J.; Scandolâra, J. E.; and Rizzotto, G. R. 2004*b*. Significance of the Nova Brasilândia metasedimentary belt in western Brazil: redefining the Mesoproterozoic boundary of the Amazon craton. Tectonics v. 23 TC 6004; doi: 10.1028/2003TC001563.

Tohver, E.; van der Pluijm, B. A.; Mezger, K.; Scandolâra, J. E.; and Essene, E. J. 2005. Two-stage tectonic history of the SW Amazon craton in the late Mesoproterozoic: identifying a cryptic suture zone. Precambrian Res., forthcoming.

Tohver, E.; van der Pluijm, B. A.; Van der Voo, R.; Rizzotto, G.; and Scandolâra, J. E. 2002. Paleogeography of the Amazon craton at 1.2 Ga: early Grenvillian collision with the Llano segment of Laurentia. Earth Planet. Sci. Lett. 199:185–200.

Van Schmus, W. R.; Bickford, M. E.; and Turek, A. 1996. Proterozoic geology of the east-central mid-continent basement. *In* van der Pluijm, B. A., and Catacosinos, P. A., eds. Basement and basins of eastern North America. Geol. Soc. Am. Spec. Pap. 308:7–32.

Voll, G.; Evangelakakis, C.; and Kroll, H. 1994. Revised two-feldspar thermometry applied to Sri Lankan feldspars. Precambrian Res. 66:351–377.

Walker, N. 1992. Middle Proterozoic geologic evolution of Llano uplift, Texas: evidence from U-Pb zircon geochronometry. Geol. Soc. Am. Bull. 104:494–504.

Weil, A. B.; Van der Voo, R.; MacNiocaill, C.; and Meert,

J. G. 1998. The Proterozoic supercontinent Rodinia: paleomagnetically derived reconstruction for 1100 to 800 Ma. Earth Planet. Sci. Lett. 154:13–24.

Wen, S., and Nekvasil, H. 1994. SOLVCALC: an interactive graphics program package for calculating the ternary feldspar solvus and for two-feldspar geothermometry. Comput. Geosci. 20:1025–1040.

White, D. J.; Easton, R. M.; Culshaw, N. G.; Milkereit, B.; Forsyth, D. A.; Carr, S.; Green, A. G.; and Davidson, A. 1994. Seismic images of the Grenville Orogen in Ontario: the Abitibi-Grenville lithoprobe transect seismic reflection results. I. The western Grenville Province and Pontiac Subprovince. Can. J. Earth Sci. 31:293–307.

Whitehouse, M. J., and Platt, J. P. 2003. Dating high-grade metamorphism: constraints from rare-earth elements in zircon and garnet. Contrib. Mineral. Petrol. 145: 61–74.

Wilkerson, A.; Carlson, W. D.; and Smith, D. 1988. High pressure metamorphism during the Llano orogeny inferred from Proterozoic eclogite remnants. Geology 16:391–394.

© 2005 by The University of Chicago. All rights reserved.

Appendix C from E. Tohver et al., "Late Mesoproterozoic Deformation of SW Amazonia (Rondônia, Brazil): Geochronological and Structural Evidence for Collision with Southern Laurentia"

(J. Geol., vol. 113, no. 3, p. 309)

$^{40}Ar/^{39}Ar$ Techniques and Isotopic Data

Hornblende grains were checked for compositional zoning and intergrowths with cummingtonite or actinolite using the electron microprobe in energy-dispersive mode. Euhedral, unaltered grains of hornblende ranging in size from 375 to 850 μm were selected by hand with a binocular microscope. Samples consisting of 10–15 grains were weighed and packaged in foil at the University of Michigan Radiogenic Isotope Geochemistry Laboratory. Samples were irradiated for 10–14 d at the University of Michigan Ford Phoenix Reactor. Neutron fluxes were monitored with samples of the Mmhb-1 standard using an age of 520.4 Ma (Samson and Alexander 1987). Single grains were step-heated using a defocused argon-ion laser until the grain was completely fused. Nonargon components were extracted using two 1/s SAES getters (ST101 alloy) and a liquid N_2 cold finger. Argon isotopic ratios were measured with a mass spectrometer (Mass Analyzer Products 215) with a Niers source and Balzer electron multiplier. Extraction line blanks were run after every 10 heating steps. Duplicates were run on all samples to determine grain-to-grain variability and reproducibility of results. Plateau ages were calculated as the inverse mean of ages from individual increments in the plateau, with a plateau defined by five or more consecutive steps containing >50% of ^{39}Ar whose errors overlap at the 2σ level (fig. C1). Where compositional differences are clearly responsible for disturbances in the age spectra or plateaus are not otherwise clear, only the total gas age is reported.

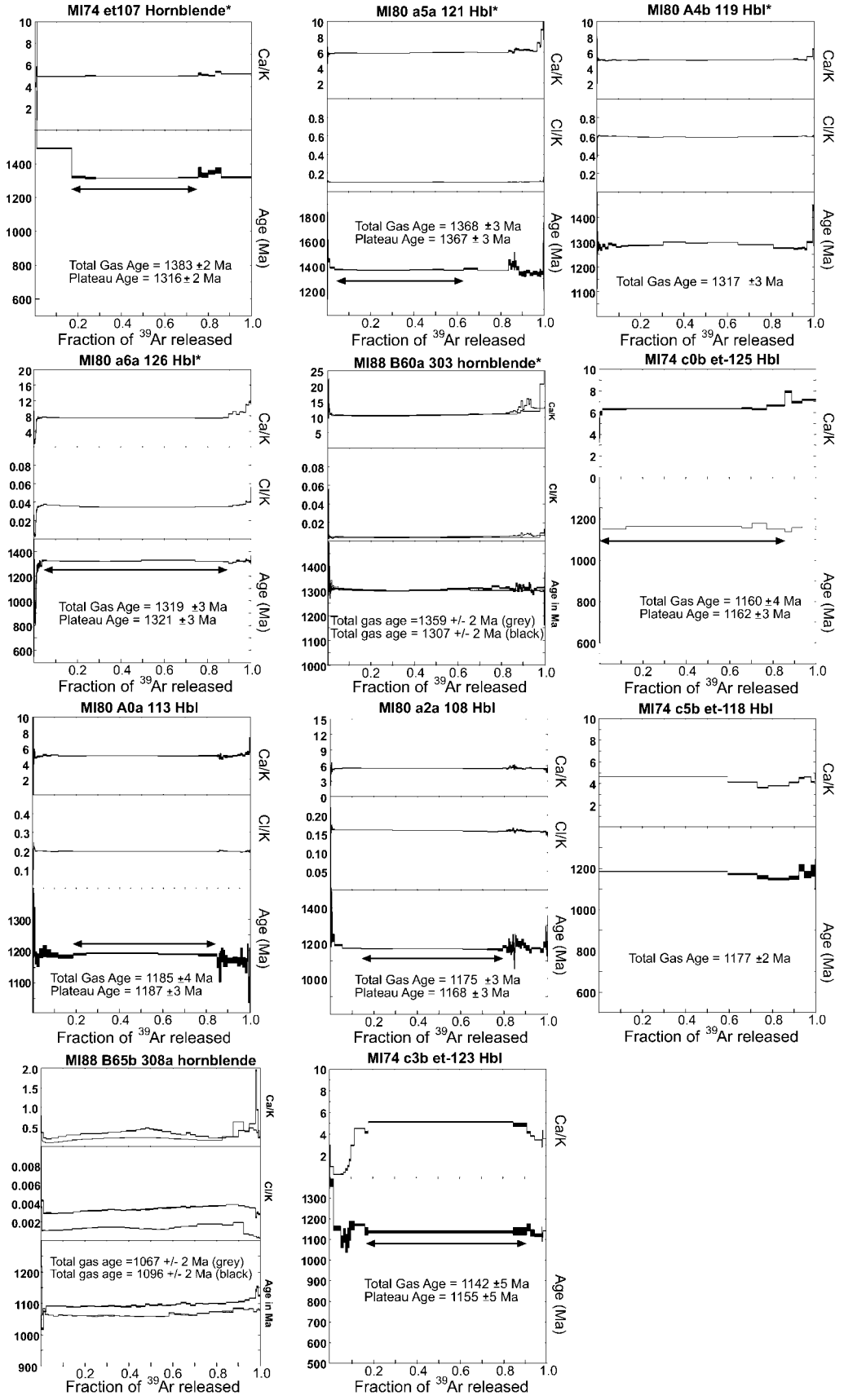
MI74 et107 Hornblende*
Total Gas Age = 1383 ±2 Ma
Plateau Age = 1316 ± 2 Ma
MI80 a5a 121 Hbl*
Total Gas Age = 1368 ±3 Ma
Plateau Age = 1367 ± 3 Ma
MI80 A4b 119 Hbl*
Total Gas Age = 1317 ±3 Ma
MI80 a6a 126 Hbl*
Total Gas Age = 1319 ±3 Ma
Plateau Age = 1321 ±3 Ma
MI88 B60a 303 hornblende*
Total gas age =1359 +/- 2 Ma (grey)
Total gas age = 1307 +/- 2 Ma (black)
MI74 c0b et-125 Hbl
Total Gas Age = 1160 ±4 Ma
Plateau Age = 1162 ±3 Ma
MI80 A0a 113 Hbl
Total Gas Age = 1185 ±4 Ma
Plateau Age = 1187 ±3 Ma
MI80 a2a 108 Hbl
Total Gas Age = 1175 ±3 Ma
Plateau Age = 1168 ± 3 Ma
MI74 c5b et-118 Hbl
Total Gas Age = 1177 ±2 Ma
MI88 B65b 308a hornblende
Total gas age =1067 +/- 2 Ma (grey)
Total gas age = 1096 +/- 2 Ma (black)
MI74 c3b et-123 Hbl
Total Gas Age = 1142 ±5 Ma
Plateau Age = 1155 ±5 Ma
Ca/K
Cl/K
Age (Ma)
Age in Ma
Fraction of 39Ar released

Figure C1. Age spectra from $^{40}Ar/^{39}Ar$ analysis of hornblende samples. Sample names followed by an asterisk denote hornblende grains separated from shear zone samples. Note that the Ca/K and Cl/K ratios are generally plateau-like until the final fusion steps, suggestive of relatively homogeneous hornblende. Compositions deduced from these ratios are similar for both shear zone and duplex block samples, suggesting that mineralogical differences (i.e., the presence of actinolite in shear zone amphiboles) cannot account for the different ages.

© 2005 by The University of Chicago. All rights reserved.

Appendix B from E. Tohver et al., "Late Mesoproterozoic Deformation of SW Amazonia (Rondônia, Brazil): Geochronological and Structural Evidence for Collision with Southern Laurentia"

(J. Geol., vol. 113, no. 3, p. 309)

Geochronological Sample Descriptions and Analytical Techniques

Table B1
Geochronological Sample Descriptions and Analytical Techniques

Sample	Location (lat., long.)	Sample description	Mineral assemblage	40Ar/39Ar, Hbl total gas age	40Ar/^{39}Ar, Hbl plateau
108	9°58.51′S, 63°2.24′W	Quarry outcrop; strong NS foliation in Serra de Previdencia suite, granite with subordinate charnockite, some igneous features preserved	Perthitic Kspar with antiperthitic Plag; Opx (Fs_{90}) rimmed by Bio/Z/Ap/Al/Mag/Hem/Ilm/Hbl; Mag overgrown by titanite	1168 ± 3	1175 ± 3
113	10°9.143′S, 62°50.54′W	Uniao Massif-sheared rapakivi suite; zircon age of 1.35 Ga reported by Bettencourt et al. (1999); protomylonitic augen gneiss; subvertical lineation defined by stretched feldspar	Large clasts of perthitic and antiperthitic feldspars in recrystallized matrix; Bio/Hbl/Plag/Ksp/Ilm/Z/Ap/Al; Mag inclusions in Hbl (originally igneous pyroxene?)	1185 ± 4, 1161 ± 4	1188 ± 5
118	10°17.75′S, 62°46.26′W	Migmatite with injections of undeformed Kspar-rich leucosomes; Hbl/Garnet in recrystallized matrix; steep foliation strikes N 20° E	Poikiloblastic, unzoned garnet ($Alm_{72}Grs_5Pyr_{19}Sps_3$)/Bio/Plag/Kspar/Qtz/Z/Mon/Hbl; no oxides present	1245 ± 2, 1177 ± 2	
119	10°22.262′S, 62°33.48′W	Roadcut; dark green charnockite, extremely dense; deformed feldspar-rich pods	Gar/Opx/Cpx/Hbl/Kspar/Mag/Ap/Cc/Qtz; >20% oxides ilmenite; no Plag; Hbl strained with cataclastic rims, large unzoned garnet	1356 ± 3, 1317 ± 3	
121	10°31.85′S, 62°23.86′W	Road outcrop; vertical foliation 235/70NW; mafic dikes affected by high-grade folding; greenish rock with garnet	Gar/nonperthitic Kspar/Plag/Qtz/Bio/Z/Chl	1367 ± 3, 1328 ± 3	1367 ± 3

Table B1 (*Continued*)

Sample	Location (lat., long.)	Sample description	Mineral assemblage	40Ar/39Ar, Hbl total gas age	40Ar/^{39}Ar, Hbl plateau
123	10°42.52′S, 62°15.38′W	Massive, garnetiferous charnockite from within duplex; weak foliation formed by amphibole, 203/75W; U-Pb zircon 1.35–1.55 Ga (Bettencourt et al. 1999)	Garnet rimming Plag, HbL, Opx Hbl/Opx/ Ilm/Plag/Kspar/Qtz/ All/FeS/Cc/Ap	1142 ± 5, 1243 ± 3	1155 ± 5
125	11°9.41′S, 61°54.01′W	Partially mylonitized Serra de Previdencia granitoid; shear zones 180/75W; lineation plunges 15 to N; shear zone with well-developed C-C′ fabric, sigma clasts showing sinistral offset; rare igneous textures preserved	Spessartine-rich Gar with Ep inclusions; both recrystallized Kspar/ Plag and relict igneous grains with perthitic texture; Qtz/Bio/Hbl/ Chl/Ap/All/Z	1310 ± 5	1190 ± 6
126	11°10.93′S, 61°54.17′W	Banded garnet-amphibolite gneiss partially migmatized with large Plag-rich leucosomes; axial plane of chief fold set 330/90	Large garnet, strongly zoned with Grs-rich, low-Mg# rims inclusions of Ep/Qtz/ Plag/Hbl/Ap/Kspar/Al/ Bio/Chl/Ti-mag/hem/ mon/ep; matrix foliation defined by biotite	1318 ± 3, 1348 ± 3	1325 ± 4, 1335 ± 5
303	9°47.78′S, 62°55.60′W	Partially migmatized outctop with igneous foliation defined by aligned large feldspar grains	Hbl/mesoperthite/ antiperthite/Qtz/Al/ Mag/Hem/Ilm/Z	1307 ± 2	
308	10°24.85′S, 62°30.36′W	Sheared sillimanite gneiss with foliation 290/70N	Gar/Hbl/Bio/Sill/Ilm/Qtz/ Kspar/Plag	1067 ± 2, 1096 ± 2	
314	11°24.05′S, 61°19.25′W	Outcrop in field near amphibolitized mafic intrusion; foliation partly formed by Hbl and Bio, aligned with regional NNW/SSE trend	Hbl/Bio/Kspar/Plag/Z/Ti-Mag/Ilm	1161 ± 5, 1299 ± 5	

Note. Al = allanite, Ap = apatite, Bio = biotite, Cc = calcite, Chl = chlorite, Ep = epidote, Gar = garnet, Hbl = hornblende, Hem = hematite, Ilm = ilmenite, Kspar = K-feldspar, Mag = magnetite, Mon = monazite, Plag = plagioclase, Qtz = quartz, Sill = sillimanite, Z = zircon.

© 2005 by The University of Chicago. All rights reserved.

Appendix A from E. Tohver et al., "Late Mesoproterozoic Deformation of SW Amazonia (Rondônia, Brazil): Geochronological and Structural Evidence for Collision with Southern Laurentia"

(J. Geol., vol. 113, no. 3, p. 309)

Feldspar Thermometry Methods

The determination of the preexsolution compositions of coexisting feldspar pairs is undertaken by reintegration of the individual exsolved feldspar grains (Bohlen and Essene 1977). Two different electron microprobe analytical methods were used to recover the original composition of exsolved feldspars for solvus thermometry: point analyses (3 × 3 μm) with reintegration by density-corrected image analysis (average of 100 spot analyses per grain; two feldspar pairs per sample) and grain transects by open beam (15 × 15 μm) analysis (20–75 analyses per grain; two feldspar pairs per sample). Microprobe operating conditions were the same for both techniques, with accelerating potential set at 15 keV and a sample current of 10 nA, to minimize Na volatilization. Calibration was carried out with mineral standards with sample analyses conducted for 30 s in wavelength dispersive mode. Where exsolved lamellae are sufficiently thick for point analyses, the first technique is preferred because of the bias introduced from faulty ZAF corrections based on an inhomogeneous matrix (Bohlen and Essene 1977). Apparent disequilibrium between feldspar pairs is common, as noted by many authors (Fuhrman and Lindsley 1988; Kroll et al. 1993; Voll et al. 1994; Raase 1998) because of late-stage K-Na exchange between plagioclase and K-feldspar (Kroll et al. 1993). Compositions were corrected for this late cation exchange by allowing a variance of ≤2 mol% X_{Or} and X_{Ab} (i.e., within microprobe analytical error) and assuming constant X_{An}^{Pl} and X_{An}^{Ksp} using the SOLVCALC program (Fuhrman and Lindsley 1988; Wen and Nekvasil 1994), a process that yielded more concordant temperatures (i.e., $T_{An} \approx T_{Or} \approx T_{Ab}$). Temperatures have an uncertainty of ~75°C based on errors in the Margules parameters for feldspar and analytical uncertainty from the reintegration technique. In samples yielding discordant temperatures ($T_{Ab} \neq T_{Or} \neq T_{An}$), the T_{Ab} is considered the most reliable because it is controlled by the slope of coexisting feldspar tie lines, as opposed to the plagioclase content of matrix K-feldspar (T_{An}) or the K-feldspar content of matrix plagioclase (T_{Or}), both of which are subject to greater analytical uncertainty (Kroll et al. 1993; Raase 1998).

© 2005 by The University of Chicago. All rights reserved.

Appendix D from E. Tohver et al., "Late Mesoproterozoic Deformation of SW Amazonia (Rondônia, Brazil): Geochronological and Structural Evidence for Collision with Southern Laurentia"

(J. Geol., vol. 113, no. 3, p. 309)

Argon Isotope Data from Analyzed Samples

Table D1
Argon Isotope Data from Analyzed Samples

Step	Fraction	$^{40}Ar/^{39}Ar$	$^{38}Ar/^{39}Ar$	$^{37}Ar/^{39}Ar$	$^{36}Ar/^{39}Ar$	$^{40}Ar^{*}/^{39}Ar$	% atm	Ca/K	Age (Ma)	1σ error
Sample et107 hornblende:										
c6b-100	.002	260.363	.800	2.188	.058	243.162	6.606	2.188	3360	48
c6b-200	.004	282.771	.634	2.285	.073	261.335	7.581	2.285	3471	38
c6b-275	.004	165.410	1.672	3.102	.004	164.153	.760	3.102	2781	58
c6b-350	.161	57.832	1.796	2.697	.001	57.430	.694	2.697	1491	3
c6b-360	.061	48.051	1.760	2.688	−.001	48.271	−.458	2.688	1321	7
c6b-370	.049	47.809	1.787	2.733	−.001	47.981	−.359	2.733	1316	6
d6b-475	.380	48.089	1.782	2.710	.000	8.006	.172	2.710	1316	1
d6b-550	.093	48.487	1.798	2.728	.001	48.153	.690	2.728	1319	4
c6b-575	.015	49.545	1.815	2.820	−.001	49.849	−.613	2.820	1352	29
c6b-650	.031	48.844	1.803	2.765	.000	48.880	−.073	2.765	1333	14
c6b-750	.032	49.054	1.790	2.743	−.002	49.758	−1.436	2.743	135	13
c6b-1000	.026	50.067	1.839	2.925	−.001	50.340	−.545	2.925	1361	17
c6b-3000	.142	48.285	1.755	2.826	.000	48.201	.174	2.826	1320	4
J value = .022373 ± .00004419										
Total gas age = 1383 ± 2 Ma										
Plateau age = 1316 ± 2 Ma										
Sample et123 hornblende:										
c3b-100	.004	91.177	1.837	1.570	.122	55.111	39.556	1.570	1452	76
c3b-200	.015	57.091	.050	.556	.021	50.920	10.810	.556	1374	19
c3b-300	.033	39.995	.019	.152	.000	39.937	.147	.152	1154	11
c3b-301	.012	37.811	.017	.175	.003	36.933	2.321	.175	1089	28
c3b-325	.010	38.823	.028	.266	.002	38.326	1.281	.266	1119	33
c3b-350	.009	38.653	.044	.402	.007	36.582	5.358	.402	1081	45
c3b-375	.008	39.275	.063	.571	.005	37.754	3.872	.571	1107	47
c3b-400	.008	39.225	.103	.885	−.001	39.416	−.485	.885	1143	47
c3b-450	.015	40.773	.251	1.614	.001	40.575	.488	1.614	1168	23
c3b-500	.049	40.573	.402	2.465	.000	40.720	−.363	2.465	1171	6
c3b-550	.016	39.075	.371	2.271	−.001	39.265	−.488	2.271	1140	19
c3b-600	.668	39.013	.459	2.790	.000	39.069	−.143	2.790	1135	6
c3b-605	.063	38.849	.457	2.658	−.001	39.260	−1.59	2.658	1140	18
c3b-620	.018	38.912	.373	2.272	−.004	40.143	−3.165	2.272	1158	17
c3b-67	.018	38.397	.342	2.083	−.002	38.853	−1.187	2.83	1131	17
c3b-750	.032	38.352	.304	1.897	.000	38.314	.101	1.897	1119	8
c3b-780	.001	38.253	.259	1.594	−.004	39.440	−3.11	1.594	1143	18
c3b-850	.001	38.371	.249	1.541	.001	37.990	.992	1.541	1112	23
c3b-1000	.004	38.440	.372	2.348	.001	38.188	.655	2.348	1116	7
c3b-3000	.015	39.320	.311	1.951	.000	39.369	−.124	1.951	1142	2
J value = .022432 ± .0000538										
Total gas age = 1142 ± 5 Ma										
Plateau age = 1155 ± 5 Ma										
Sample et119 hornblende:										

Table D1 (*Continued*)

Step	Fraction	$^{40}Ar/^{39}Ar$	$^{38}Ar/^{39}Ar$	$^{37}Ar/^{39}Ar$	$^{36}Ar/^{39}Ar$	$^{40}Ar^{*}/^{39}Ar$	% atm	Ca/K	Age (Ma)	1σ error
a4b-100	.000	4406.852	1.036	4.649	.047	4392.940	.316	4.649	9498	75
a4b-200	.000	283.946	1.386	4.983	.125	246.932	13.036	4.983	4455	108
a4b-250	.000	151.077	.942	5.823	.221	85.625	43.324	5.823	2811	204
a4b-300	.000	51.434	.742	6.561	.030	42.588	17.198	6.561	1899	192
a4b-350	.000	174.386	.945	3.703	.028	166.129	4.735	3.703	3813	72
a4b-400	.000	49.056	1.056	4.980	.023	42.204	13.967	4.980	1889	147
a4b-425	.000	27.184	1.382	3.358	−.044	40.234	−48.07	3.358	1833	231
a4b-450	.000	32.014	1.701	5.613	.048	17.744	44.577	5.613	1037	537
a4b-475	.000	31.969	1.589	3.553	−.044	44.929	−4.538	3.553	1963	388
a4b-500	.000	30.699	1.886	1.887	−.045	44.087	−43.61	1.887	1940	196
a4b-525	.000	34.125	2.074	3.460	−.021	40.354	−18.254	3.46	1836	226
a4b-550	.000	24.772	2.217	3.291	−.005	26.326	−6.27	3.291	1384	274
a4b-575	.000	23.851	2.431	2.753	−.011	27.105	−13.643	2.753	1412	149
a4b-60	.001	27.277	2.497	3.090	−.007	29.471	−8.43	3.090	1495	103
a4b-625	.001	24.697	2.795	2.792	.002	24.150	2.215	2.792	1302	42
a4b-650	.002	23.756	2.861	2.770	.001	23.594	.684	2.770	1280	26
a4b-675	.004	23.511	2.885	2.781	.000	23.643	−.562	2.781	1282	18
a4b-700	.006	23.740	2.886	2.741	.000	23.621	.500	2.741	1281	10
a4b-725	.009	23.515	2.875	2.749	.000	23.378	.585	2.749	1272	7
a4b-750	.012	23.729	2.867	2.741	.000	23.735	−.026	2.741	1286	5
a4b-775	.015	23.549	2.869	2.693	.000	23.486	.266	2.693	1276	5
a4b-800	.017	23.969	2.866	2.725	.000	23.906	.260	2.725	1292	4
a4b-825	.020	23.775	2.871	2.750	.000	23.787	−.048	2.750	1288	4
a4b-850	.022	23.544	2.863	2.716	.000	23.585	−.173	2.716	1280	3
a4b-875	.032	23.696	2.851	2.743	.000	23.667	.120	2.743	1283	2
a4b-900	.042	23.627	2.831	2.732	.000	23.766	−.587	2.732	1287	2
a4b-925	.054	23.689	2.821	2.760	.000	23.735	−.195	2.760	1286	2
a4b-950	.065	23.748	2.815	2.732	.000	23.789	−.171	2.732	1288	1
a4b-975	.103	24.067	2.820	2.731	.000	24.090	−.095	2.731	1300	1
a4b-1000	.101	23.989	2.817	2.723	.000	23.984	.022	2.723	1295	1
a4b-1050	.140	24.047	2.815	2.735	.000	24.062	−.062	2.735	1298	1
a4b-1100	.162	23.801	2.832	2.741	.000	23.821	−.083	2.742	1289	0
a4b-1150	.093	23.437	2.847	2.786	.000	23.473	−.156	2.786	1276	1
a4b-1200	.019	23.324	2.846	2.806	.000	23.389	−.277	2.806	1272	3
a4b-1300	.019	23.365	2.856	2.768	.000	23.433	−.293	2.768	1274	3
a4b-1400	.012	23.392	2.880	2.761	.000	23.509	−.499	2.761	1277	4
a4b-1500	.011	23.411	2.864	2.736	.000	23.353	.247	2.736	1271	5
a4b-1750	.027	24.034	2.832	2.973	.000	24.096	−.259	2.973	1300	3
a4b-2000	.003	28.477	2.886	3.509	.002	27.802	2.372	3.509	1437	13
a4b-2250	.002	24.044	2.827	2.846	.000	24.127	−.347	2.846	1301	17
a4b-2500	.001	23.981	2.861	2.800	.000	23.952	.119	2.800	1294	43
a4b-3000	.000	22.744	2.882	3.138	.033	13.055	42.598	3.138	816	199
a4b-3500	.000	47.568	2.561	2.075	.042	35.239	25.918	2.075	1684	558
a4b-4000	.000	26.007	2.839	1.599	−.032	35.547	−36.684	1.599	1694	427
J value = .0438 ± .000143										
Total gas age = 1317 ± 3 Ma										
Sample et108 hornblende:										
a2a-100	.000	43.593	1.207	4.738	−.025	51.008	−17.011	4.738	2121	303
a2a-200	.001	69.717	.320	4.456	.112	36.606	47.493	4.456	1730	258
a2a-250	.000	28.758	.332	3.075	−.058	45.914	−59.658	3.075	1992	255
a2a-300	.001	23.991	.402	2.008	−0.013	27.838	−16.036	2.008	1441	264
a2a-350	.001	24.505	.373	1.568	−.035	34.944	−42.598	1.568	1678	288
a2a-400	.001	23.364	.493	2.320	−.024	30.552	−30.769	2.320	1536	203
a2a-425	.001	27.650	.619	2.055	−.029	36.261	−31.142	2.055	1719	265
a2a-450	.001	26.712	.754	2.623	.005	25.180	5.735	2.623	1344	166
a2a-475	.001	25.660	.784	2.880	−.004	26.826	−4.544	2.880	1405	142
a2a-500	.001	24.999	.802	3.304	−.001	25.230	−.925	3.304	1346	144
a2a-525	.002	22.857	.786	2.760	−.004	23.950	−4.778	2.760	1297	79
a2a-550	.009	22.022	.769	2.857	−.001	22.232	−.955	2.857	1229	22
a2a-575	.037	21.170	.764	2.950	.000	21.210	−.190	2.950	1188	5
a2a-600	.087	20.812	.764	3.005	.000	20.797	.072	3.005	1171	2

Table D1 (*Continued*)

Step	Fraction	$^{40}Ar/^{39}Ar$	$^{38}Ar/^{39}Ar$	$^{37}Ar/^{39}Ar$	$^{36}Ar/^{39}Ar$	$^{40}Ar^{*}/^{39}Ar$	% atm	Ca/K	Age (Ma)	1σ error
a2a-625	.143	20.726	.764	2.995	.000	20.720	.026	2.995	1168	2
a2a-650	.323	20.747	.756	2.993	.000	20.754	−.036	2.993	1169	1
a2a-675	.113	20.682	.750	2.940	.000	20.630	.250	2.940	1164	3
a2a-700	.049	20.623	.743	2.950	.000	20.638	−.076	2.950	1164	4
a2a-725	.021	20.774	.747	2.959	.001	20.591	.881	2.959	1162	7
a2a-750	.016	20.937	.750	3.001	.000	21.006	−.332	3.001	1180	7
a2a-775	.009	20.868	.755	2.933	.001	20.607	1.251	2.933	1163	17
a2a-800	.005	20.679	.760	3.039	−.002	21.176	−2.404	3.039	1187	41
a2a-825	.005	20.920	.757	3.179	.000	20.973	−.254	3.179	1178	30
a2a-850	.006	20.740	.759	3.032	.000	20.593	.710	3.032	1162	27
a2a-875	.005	20.820	.759	3.094	.000	20.936	−.555	3.094	1177	29
a2a-900	.003	21.220	.775	3.173	−.001	21.576	−1.680	3.173	1203	47
a2a-925	.003	21.206	.748	2.968	−.006	23.092	−8.895	2.968	1264	50
a2a-950	.003	21.006	.744	3.245	.005	19.432	7.495	3.245	1113	58
a2a-975	.003	20.878	.735	2.897	−.002	21.490	−2.929	2.897	1199	52
a2a-1000	.004	21.263	.751	3.101	−.002	21.784	−2.450	3.101	1211	32
a2a-1050	.006	20.973	.766	2.992	−.002	21.561	−2.803	2.992	1202	22
a2a-1100	.010	21.258	.760	2.983	.000	21.349	−.430	2.983	1194	16
a2a-1150	.008	21.318	.762	2.993	.000	21.267	.239	2.993	1190	20
a2a-1200	.010	21.335	.755	2.916	−.001	21.607	−1.273	2.916	1204	18
a2a-1300	.009	21.403	.751	2.890	.001	21.177	1.058	2.890	1187	14
a2a-1400	.016	21.070	.742	3.015	.001	20.847	1.057	3.015	1173	14
a2a-1500	.010	20.824	.746	3.025	.001	20.386	2.103	3.025	1154	13
a2a-1750	.039	20.767	.748	2.951	.000	20.806	−.189	2.951	1171	5
a2a-2000	.016	20.736	.739	2.947	.001	20.483	1.218	2.947	1158	11
a2a-2250	.009	21.372	.743	2.901	.000	21.274	.458	2.901	1191	16
a2a-2500	.003	22.610	.738	2.853	.001	22.420	.841	2.853	1237	57
a2a-3000	.002	22.793	.714	2.649	−.002	23.502	−3.111	2.649	1280	69
a2a-3500	.004	21.428	.728	2.853	.003	20.652	3.624	2.853	1165	39
a2a-4000	.001	22.433	.703	2.802	.001	22.116	1.414	2.802	1225	128
J value = .043935 ± .000161										
Total gas age = 1175 ± 3 Ma										
Plateau age = 1168 ± 3 Ma										
Sample et121 hornblende:										
a5a-100	.000	24.260	1.833	5.288	.108	−7.722	131.831	5.288	−742	1032
a5a-200	.000	24.228	.468	36.485	.185	−30.454	225.697	36.485	−9989	4169
a5a-250	.000	30.841	.572	20.776	.417	−92.240	399.082	20.776	−18485	1380
a5a-300	.000	31.452	.568	30.344	.234	−37.625	219.629	30.344	−21602	3166
a5a-350	.000	25.915	.331	7.343	.214	−37.465	244.571	7.343	−21240	2670
a5a-400	.000	30.162	.569	2.256	.038	19.079	36.747	2.256	1093	1273
a5a-425	.000	17.116	1.098	.080	.030	8.211	52.029	.080	553	3494
a5a-450	.000	41.189	.731	3.504	−.079	64.567	−56.757	3.504	2418	883
a5a-475	.000	41.977	.733	4.087	.000	41.836	.337	4.087	1875	787
a5a-500	.001	31.899	.612	3.398	.009	29.348	7.997	3.398	1488	259
a5a-525	.001	29.836	.532	3.253	.008	27.473	7.921	3.253	1422	293
a5a-550	.001	29.458	.500	2.880	−.023	36.275	−23.139	2.880	1713	121
a5a-575	.001	27.910	.525	2.837	−.026	35.609	−27.581	2.837	1692	99
a5a-600	.002	27.298	.535	3.116	−.012	30.980	−13.485	3.116	1544	68
a5a-625	.007	26.441	.494	3.159	−.006	28.138	−6.416	3.159	1446	15
a5a-650	.021	26.123	.488	3.179	−.001	26.504	−1.459	3.179	1387	6
a5a-675	.038	25.798	.483	3.207	−.001	26.089	−1.126	3.207	1372	6
a5a-700	.064	25.822	.482	3.217	−.001	25.999	−.687	3.217	1369	3
a5a-725	.126	25.970	.484	3.203	.000	25.921	.190	3.203	1366	2
a5a-750	.119	25.929	.480	3.201	.000	25.946	−.065	3.201	1367	3
a5a-775	.106	25.984	.483	3.231	.000	25.975	.035	3.231	1368	2
a5a-800	.050	26.106	.490	3.244	.000	26.092	.056	3.244	1372	4
a5a-825	.093	25.873	.483	3.240	.000	25.945	−.277	3.240	1367	2
a5a-850	.064	26.009	.488	3.271	−.001	26.232	−.861	3.271	1377	5
a5a-875	.141	25.757	.487	3.240	.000	25.839	−.319	3.240	1363	2
a5a-900	.009	26.294	.492	3.364	−.005	27.680	−5.272	3.364	1430	23
a5a-925	.008	26.087	.476	3.343	−.002	26.762	−2.587	3.343	1397	27

Table D1 (*Continued*)

Step	Fraction	$^{40}Ar/^{39}Ar$	$^{38}Ar/^{39}Ar$	$^{37}Ar/^{39}Ar$	$^{36}Ar/^{39}Ar$	$^{40}Ar^{*}/^{39}Ar$	% atm	Ca/K	Age (Ma)	1σ error
a5a-950	.009	26.023	.486	3.244	−.004	27.259	−4.750	3.244	1415	24
a5a-975	.004	25.990	.488	3.374	−.007	27.915	−7.407	3.374	1438	70
a5a-1000	.008	25.827	.486	3.484	−.005	27.276	−5.609	3.484	1415	27
a5a-1050	.011	26.249	.489	3.481	.000	26.341	−.348	3.481	1381	15
a5a-1100	.013	25.360	.500	3.411	.001	25.207	.602	3.411	1339	15
a5a-1150	.010	25.647	.484	3.425	.002	25.111	2.093	3.425	1336	20
a5a-1200	.010	25.700	.488	3.456	.002	25.110	2.297	3.456	1336	21
a5a-1300	.017	25.952	.496	3.434	.001	25.641	1.197	3.434	1356	11
a5a-1400	.015	25.224	.518	3.391	.001	25.067	.623	3.391	1334	13
a5a-1500	.019	25.452	.501	3.338	.000	25.356	.377	3.338	1345	15
a5a-1750	.012	25.370	.508	3.932	.001	25.110	1.024	3.932	1336	17
a5a-2000	.005	24.340	.549	3.690	−.003	25.318	−4.021	3.690	1343	31
a5a-2250	.011	25.483	.518	4.833	.000	25.338	.569	4.833	1344	13
a5a-2500	.002	25.909	.588	14.567	−.013	29.847	−15.196	14.567	1505	85
a5a-2500	.001	26.978	.706	22.808	−.014	31.234	−15.774	22.808	1552	199
a5a-4000	.001	27.077	.525	4.507	.008	24.815	8.354	4.507	1325	113
J value = .043675 ± .000129										
Total gas age = 1368 ± 3 Ma										
Plateau age = 1367 ± 3 Ma										
Sample et126 hornblende:										
a6a-100	.000	97.557	6.284	4.421	.208	36.098	62.999	4.421	1705	184
a6a-200	.000	26.303	3.242	1.875	.019	20.719	21.229	1.875	1161	100
a6a-250	.001	17.162	.120	.685	.025	9.918	42.212	.685	648	97
a6a-300	.001	13.723	.027	.885	.009	10.945	20.245	.885	703	76
a6a-350	.001	24.874	.031	.608	.005	23.353	6.116	.608	1266	71
a6a-400	.001	17.302	.030	.933	.009	14.591	15.672	.933	888	44
a6a-425	.001	15.205	.015	.577	.003	14.175	6.776	.577	868	49
a6a-450	.001	16.089	.017	.607	.002	15.404	4.257	.607	926	66
a6a-475	.001	15.193	.017	.952	.000	15.148	.301	.952	914	73
a6a-500	.001	15.390	.021	1.189	.004	14.259	7.350	1.189	872	70
a6a-525	.001	15.932	.042	1.502	−.004	17.020	−6.829	1.502	1001	55
a6a-550	.001	16.410	.052	1.611	−.005	17.764	−8.248	1.611	1034	52
a6a-575	.001	18.077	.092	2.198	−.003	19.081	−5.559	2.198	1092	79
a6a-600	.001	19.053	.110	2.751	.006	17.189	9.782	2.751	1009	71
a6a-625	.001	20.729	.130	2.977	.001	20.370	1.734	2.977	1146	61
a6a-650	.001	21.565	.146	3.773	.001	21.307	1.195	3.773	1185	42
a6a-675	.002	23.208	.152	3.763	.002	22.491	3.091	3.763	1232	29
a6a-700	.002	22.967	.153	3.942	−.001	23.165	−.861	3.942	1259	31
a6a-725	.002	23.934	.166	4.002	.002	23.408	2.199	4.002	1268	32
a6a-750	.003	24.661	.167	4.199	.004	23.447	4.924	4.199	1270	25
a6a-775	.004	24.568	.169	4.001	.002	23.889	2.766	4.001	1287	21
a6a-800	.004	24.628	.170	4.097	.001	24.409	.887	4.097	1307	20
a6a-825	.003	24.236	.171	4.143	.000	24.190	.191	4.143	1299	22
a6a-850	.005	24.236	.174	4.073	.001	23.830	1.675	4.073	1285	7
a6a-875	.008	25.283	.175	4.197	.001	24.971	1.234	4.197	1328	7
a6a-900	.014	25.251	.181	4.228	.001	24.979	1.079	4.228	1329	6
a6a-925	.060	24.920	.175	4.135	.000	24.859	.246	4.135	1324	1
a6a-950	.091	24.790	.171	4.084	.000	24.780	.040	4.084	1321	1
a6a-975	.090	24.830	.167	4.063	.000	24.794	.145	4.063	1322	1
a6a-1000	.053	24.749	.166	4.084	.000	24.751	−.006	4.084	1320	1
a6a-1050	.141	24.797	.165	4.081	.000	24.809	−.050	4.081	1322	1
a6a-1100	.247	24.999	.166	4.077	.000	25.004	−.022	4.077	1329	3
a6a-1150	.129	24.774	.168	4.058	.000	24.768	.024	4.058	1321	1
a6a-1200	.025	24.730	.168	4.134	.000	24.687	.175	4.134	1317	2
a6a-1300	.020	24.326	.169	4.650	.000	24.307	.080	4.650	1303	3
a6a-1400	.017	24.741	.176	4.968	.000	24.595	.592	4.968	1314	4
a6a-1500	.014	25.026	.175	4.567	.000	24.890	.544	4.567	1325	6
a6a-1750	.017	24.858	.178	4.929	.000	24.800	.235	4.929	1322	3
a6a-2000	.011	24.732	.180	4.867	.000	24.749	−.067	4.867	1320	6
a6a-2250	.005	24.800	.196	5.963	−.001	25.090	−1.168	5.963	1333	7
a6a-2500	.010	24.996	.192	5.919	.000	24.961	.140	5.919	1328	5

Table D1 (*Continued*)

Step	Fraction	$^{40}Ar/^{39}Ar$	$^{38}Ar/^{39}Ar$	$^{37}Ar/^{39}Ar$	$^{36}Ar/^{39}Ar$	$^{40}Ar^{*}/^{39}Ar$	% atm	Ca/K	Age (Ma)	1σ error
a6a-3000	.009	24.851	.192	6.314	.000	24.777	.299	6.314	1321	7
a6a-3500	.002	25.260	.264	11.120	.000	25.190	.277	11.120	1336	27
a6a-4000	.000	26.707	.162	6.922	−.029	35.285	−32.116	6.922	1680	218
J value = .043573 ± .00012										
Total gas age = 1319 ± 3 Ma										
Plateau age = 1321 ± 3 Ma										
Sample et113 hornblende:										
a0a-100	.001	15.225	.398	4.630	.003	14.420	5.293	4.630	887	195
a0a-200	.001	20.886	.164	1.899	.003	20.138	3.580	1.899	1145	179
a0a-250	.000	11.030	.164	6.442	−.024	18.043	−63.575	6.442	1055	600
a0a-300	.000	10.590	.256	2.488	−.024	17.683	−66.971	2.488	1039	490
a0a-350	.000	12.022	.298	1.406	.018	6.727	44.043	1.406	468	778
a0a-400	.000	8.960	.448	1.505	.038	−2.413	126.933	1.505	−203	1540
a0a-425	.000	22.010	.556	2.499	−.225	88.569	−302.405	2.499	2867	546
a0a-450	.000	19.929	.829	−.044	−.073	41.604	−108.761	−.044	1878	1034
a0a-475	.000	22.337	.827	.454	−.031	31.603	−41.481	.454	1573	631
a0a-500	.000	17.236	.717	.557	−.098	46.312	−168.688	.557	2006	402
a0a-525	.000	22.856	1.001	5.544	−.042	35.223	−54.106	5.544	1690	666
a0a-550	.000	23.943	1.036	4.450	−.017	28.847	−20.483	4.450	1479	226
a0a-575	.001	25.292	1.104	3.046	−.005	26.661	−5.415	3.046	1401	206
a0a-600	.001	23.680	1.041	2.496	.001	23.472	.878	2.496	1281	103
a0a-625	.002	23.518	1.036	2.879	.002	22.844	2.868	2.879	1256	76
a0a-650	.003	22.493	.989	2.892	−.004	23.632	−5.066	2.892	1287	53
a0a-675	.008	21.159	.950	2.610	.001	20.876	1.339	2.610	1176	20
a0a-700	.012	21.333	.951	2.671	.002	20.692	3.003	2.671	1169	21
a0a-725	.016	21.248	.951	2.697	.000	21.246	.011	2.697	1191	15
a0a-750	.017	21.410	.944	2.799	.000	21.388	.101	2.799	1197	19
a0a-775	.020	21.135	.941	2.739	.000	21.224	−.420	2.739	1191	12
a0a-800	.032	21.104	.936	2.783	.000	21.105	−.001	2.783	1186	7
a0a-825	.069	21.066	.945	2.721	.000	20.975	.433	2.721	1180	5
a0a-850	.061	21.209	.942	2.703	.000	21.157	.243	2.703	1188	4
a0a-875	.329	21.233	.937	2.732	.000	21.232	.004	2.732	1191	1
a0a-900	.185	21.167	.934	2.711	.000	21.167	.000	2.711	1188	2
a0a-925	.085	21.105	.936	2.734	.000	21.099	.030	2.734	1185	4
a0a-950	.010	21.289	.929	2.729	.003	20.495	3.732	2.729	1160	17
a0a-975	.004	21.101	.961	2.635	.003	20.125	4.626	2.635	1145	47
a0a-1000	.004	21.013	.962	2.768	.003	20.201	3.864	2.768	1148	49
a0a-1050	.011	20.858	.957	2.574	−.001	21.095	−1.136	2.574	1185	23
a0a-1100	.007	21.326	.944	2.710	.002	20.834	2.308	2.710	1174	27
a0a-1150	.012	20.958	.945	2.669	.001	20.643	1.506	2.669	1167	19
a0a-1200	.025	20.902	.942	2.692	.001	20.684	1.042	2.692	1168	9
a0a-1300	.021	21.083	.940	2.741	.001	20.701	1.809	2.741	1169	10
a0a-1400	.014	21.188	.942	2.779	.002	20.567	2.930	2.779	1163	14
a0a-1500	.009	21.022	.920	2.836	.000	20.991	.150	2.836	1181	27
a0a-1750	.014	20.773	.925	2.759	.001	20.530	1.173	2.759	1162	16
a0a-2000	.007	21.077	.939	2.896	.003	20.269	3.836	2.896	1151	24
a0a-2250	.006	21.156	.957	2.948	.000	21.288	−.624	2.948	1193	29
a0a-2500	.005	20.821	.942	2.903	.008	18.475	11.269	2.903	1074	42
a0a-3000	.002	20.734	.944	3.669	.006	18.879	8.948	3.669	1092	116
a0a-3500	.002	21.031	.963	3.167	.008	18.544	11.822	3.167	1077	108
a0a-4000	.001	20.583	.911	3.494	.026	12.817	37.729	3.494	807	187
J value = .044037 ± .000176										
Total gas age = 1185 ± 4 Ma										
Plateau age = 1187 ± 3 Ma										
Sample et125 hornblende:										
c0b-100	.002	22.706	.895	2.260	−.072	44.047	−93.990	2.260	1242	290
c0b-200	.002	70.427	−.026	2.470	.099	41.115	41.620	2.470	1181	582
c0b-275	.011	40.912	.072	3.236	−.003	41.759	−2.069	3.236	1195	60
c0b-350	.111	39.928	.100	3.435	−.001	40.079	−.377	3.435	1159	8
c0b-400	.532	40.136	.102	3.453	.000	40.217	−.202	3.453	1162	2
c0b-410	.047	40.069	.095	3.492	−.002	40.640	−1.424	3.492	1171	15

Table D1 (*Continued*)

Step	Fraction	$^{40}Ar/^{39}Ar$	$^{38}Ar/^{39}Ar$	$^{37}Ar/^{39}Ar$	$^{36}Ar/^{39}Ar$	$^{40}Ar^{*}/^{39}Ar$	% atm	Ca/K	Age (Ma)	1σ error
c0b-430	.067	39.916	.093	3.433	−.001	40.315	−1.001	3.433	1164	14
c0b-480	.084	39.494	.096	3.634	−.002	40.085	−1.497	3.634	1159	8
c0b-530	.033	40.019	.104	4.323	.009	37.406	6.529	4.323	1101	39
c0b-630	.047	41.488	.103	3.793	.001	41.223	.641	3.793	1183	25
c0b-1500	.065	40.218	.106	3.912	.003	39.308	2.263	3.912	1143	20
J value = .022485 ± .0000643										
Total gas age = 1160 ± 4 Ma										
Plateau age = 1162 ± 3 Ma										
Sample et118 hornblende:										
c5b-625	.594	41.546	.148	2.534	.000	41.442	.252	2.534	1184	1
c5b-700	.137	40.860	.130	2.261	.000	40.846	.035	2.261	1172	4
c5b-775	.049	40.585	.121	1.988	.002	40.127	1.128	1.988	1157	9
c5b-850	.096	40.152	.124	2.061	.001	39.760	.976	2.061	1149	5
C5B-925	.045	40.437	.132	2.252	.001	40.073	.900	2.252	1156	10
C5B-1000	.025	42.132	.145	2.472	−.001	42.324	−.456	2.472	1203	16
C5B-1200	.033	41.585	.140	2.523	.003	40.743	2.024	2.523	1170	16
C5B-1500	.017	42.524	.121	2.269	.003	41.638	2.084	2.269	1189	27
C5B-3000	.005	40.515	.152	2.566	−.001	40.830	−.778	2.566	1172	72
J value = .022396 ± .0000477										
Total gas age = 1177 ± 2 Ma										
MI88-b60a 303 hornblende:										
Power:										
100	.000	36.901	.388	4.781	.087	11.252	69.507	4.781	738	210
200	.000	58.111	.189	8.196	.106	26.818	53.851	8.196	1427	171
250	.000	56.918	.070	8.759	.072	35.752	37.188	8.759	1729	125
300	.000	49.381	.058	8.832	.064	30.539	38.157	8.832	1559	125
350	.000	32.369	.047	9.173	.055	16.013	50.531	9.173	978	324
400	.000	28.025	.034	11.457	.015	23.528	16.044	11.457	1302	204
425	.000	25.908	.028	10.262	.020	20.094	22.442	10.262	1161	194
450	.000	25.414	.022	9.790	.000	25.288	.495	9.790	1370	57
475	.001	25.422	.030	8.669	−.003	26.309	−3.489	8.669	1408	88
500	.001	24.957	.028	7.717	.003	24.114	3.380	7.717	1325	44
525	.001	24.801	.023	6.864	.002	24.250	2.224	6.864	1330	30
550	.003	24.156	.023	6.410	.002	23.704	1.869	6.410	1309	12
575	.007	23.718	.022	5.884	.000	23.653	.276	5.884	1307	10
600	.016	23.640	.022	5.766	.000	23.686	−.196	5.766	1308	4
625	.041	23.683	.023	5.811	.000	23.707	−.100	5.811	1309	2
650	.087	23.586	.022	5.776	.000	23.610	−.103	5.776	1305	1
675	.107	23.551	.023	5.757	.000	23.574	−.096	5.757	1304	1
700	.139	23.469	.023	5.753	.000	23.495	−.109	5.753	1300	1
725	.143	23.491	.022	5.815	.000	23.551	−.256	5.815	1303	1
750	.096	23.646	.023	5.814	.000	23.713	−.283	5.814	1309	1
775	.067	23.680	.023	5.919	.000	23.760	−.338	5.919	1311	2
800	.042	23.619	.024	5.945	.000	23.704	−.359	5.945	1309	3
825	.034	23.803	.023	5.992	−.001	23.965	−.679	5.992	1319	3
850	.029	23.704	.024	6.025	.000	23.779	−.313	6.025	1312	2
875	.019	23.754	.025	6.160	.000	23.817	−.263	6.160	1313	5
900	.015	23.662	.026	6.331	.000	23.670	−.032	6.331	1307	5
925	.012	23.696	.028	6.552	.000	23.565	.552	6.552	1303	7
950	.008	24.015	.027	6.346	.000	24.105	−.374	6.346	1324	8
975	.006	23.644	.028	6.746	.000	23.588	.237	6.746	1304	8
1000	.003	23.612	.030	7.253	−.001	23.792	−.762	7.253	1312	16
1050	.007	23.878	.031	7.221	.000	23.952	−.311	7.221	1318	7
1100	.007	23.613	.041	8.290	.000	23.625	−.051	8.290	1306	9
1150	.009	23.654	.030	6.736	−.001	23.970	−1.334	6.736	1319	7
1200	.011	23.759	.035	7.462	.000	23.749	.039	7.462	1310	6
1300	.009	23.733	.039	8.653	.000	23.691	.178	8.653	1308	7
1400	.004	23.566	.033	7.736	−.001	23.973	−1.727	7.736	1319	15
1500	.005	23.573	.039	8.552	−.001	23.960	−1.642	8.552	1319	8
1750	.008	23.620	.031	7.136	.001	23.432	.800	7.136	1298	6
2000	.007	23.578	.026	7.120	.001	23.308	1.146	7.120	1293	9

Table D1 (*Continued*)

Step	Fraction	$^{40}Ar/^{39}Ar$	$^{38}Ar/^{39}Ar$	$^{37}Ar/^{39}Ar$	$^{36}Ar/^{39}Ar$	$^{40}Ar^{*}/^{39}Ar$	% atm	Ca/K	Age (Ma)	1σ error
2250	.012	23.662	.028	6.977	.000	23.654	.034	6.977	1307	5
2500	.036	23.876	.029	6.980	.000	23.835	.168	6.980	1314	3
3000	.002	24.115	.033	7.114	−.001	24.537	−1.753	7.114	1341	34
3500	.001	27.001	.036	8.617	.010	24.034	10.989	8.617	1322	91
4000	.000	18.453	.146	16.762	−.056	34.948	−89.393	16.762	1704	1339
J value = .044J9495 ± .000093101										
Total gas age = 1306.7 ± 2.0 Ma										
MI88-b65a 308a hornblende:										
Power:										
100	.002	28.756	.073	.423	.008	26.372	8.291	.423	1408	5
200	.003	21.934	.017	.200	.001	21.505	1.956	.200	1218	2
250	.004	18.161	.005	.080	.001	17.930	1.270	.080	1064	2
300	.009	18.431	.005	.063	.000	18.341	.489	.063	1083	1
350	.015	17.999	.005	.053	.000	17.944	.306	.053	1065	1
400	.023	17.916	.005	.051	.000	17.889	.154	.051	1063	1
425	.022	17.815	.005	.057	.000	17.810	.028	.057	1059	1
450	.021	17.905	.005	.063	.000	17.892	.068	.063	1063	1
475	.021	17.879	.005	.073	.000	17.869	.054	.073	1062	1
500	.021	17.892	.005	.081	.000	17.884	.043	.081	1062	1
525	.022	17.826	.006	.090	.000	17.823	.014	.090	1060	1
550	.023	17.841	.006	.097	.000	17.833	.042	.097	1060	1
575	.023	17.831	.006	.103	.000	17.832	−.007	.103	1060	1
600	.024	17.815	.006	.102	.000	17.817	−.013	.102	1059	1
625	.025	17.815	.007	.107	.000	17.805	.053	.107	1059	2
650	.025	17.862	.007	.107	.000	17.852	.057	.107	1061	2
675	.025	17.856	.007	.113	.000	17.852	.022	.113	1061	2
700	.025	17.842	.007	.115	.000	17.833	.051	.115	1060	2
725	.024	17.833	.007	.115	.000	17.834	−.004	.115	1060	1
750	.023	17.814	.007	.120	.000	17.813	.003	.120	1059	1
775	.022	17.832	.007	.122	.000	17.824	.047	.122	1060	1
800	.022	17.792	.006	.124	.000	17.799	−.034	.124	1058	0
825	.021	17.797	.006	.124	.000	17.785	.063	.124	1058	1
850	.020	17.786	.006	.124	.000	17.801	−.084	.124	1059	1
875	.020	17.802	.006	.125	.000	17.799	.018	.125	1058	1
900	.019	17.807	.006	.123	.000	17.806	.008	.123	1059	1
925	.019	17.801	.006	.121	.000	17.804	−.014	.121	1059	1
950	.019	17.766	.006	.120	.000	17.768	−.010	.120	1057	1
975	.019	17.797	.006	.116	.000	17.780	.091	.116	1058	1
1000	.019	17.805	.006	.114	.000	17.811	−.032	.114	1059	1
1050	.024	18.043	.006	.109	.000	18.041	.015	.109	1069	2
1100	.030	17.979	.007	.104	.000	17.971	.041	.104	1066	1
1150	.036	17.931	.007	.099	.000	17.915	.091	.099	1064	1
1200	.039	17.902	.007	.095	.000	17.887	.083	.095	1062	2
1300	.054	18.030	.008	.086	.000	18.022	.043	.086	1068	1
1400	.059	18.136	.008	.089	.000	18.129	.040	.089	1073	1
1500	.050	18.137	.008	.136	.000	18.126	.060	.136	1073	2
1750	.046	18.373	.009	.339	.000	18.371	.014	.339	1084	1
2000	.025	18.317	.003	.219	.000	18.300	.098	.219	1081	2
2250	.020	18.346	.003	.258	.000	18.339	.036	.258	1083	1
2500	.014	18.117	.002	.228	.000	18.115	.010	.228	1073	1
3000	.007	18.269	.001	.193	.000	18.258	.058	.193	1079	1
3500	.005	18.296	.002	.221	.000	18.321	−.135	.221	1082	2
4000	.007	18.244	.001	.134	.000	18.273	−.158	.134	1080	1
J value = .0448376 ± .0000799962										
Total gas age = 1066.7 ± 1.5 Ma										